

1 Permian high-temperature metamorphism in the Western Alps (NW Italy)

2

3 **Barbara E. Kunz^{a*}, Paola Manzotti^{a,b}, Brigitte von Niederhäusern^a, Martin Engi^a, James R. Darling^{a,c}, Francesco**
4 **Giuntoli^{a,d} and Pierre Lanari^a**

5

6 ^a *Institute of Geological Sciences, University of Bern, Baltzerstrasse 1+3, 3012 Bern, Switzerland*

7 ^b *Institute of Earth Sciences, University of Lausanne, Géopolis, Quartier Mouline, 1015 Lausanne, Switzerland*

8 ^c *School of Earth and Environmental Sciences, University of Portsmouth, Portsmouth, PO1 3QL, United Kingdom*

9 ^d *School of Geography, Earth and Environmental Sciences, Plymouth University, Plymouth, PL4 8AA, United Kingdom*

10

11 *Corresponding author Tel.: +41 (0)31-631 4738; fax: +41 (0)31 631 4843

12 E-mail address: barbara.kunz@geo.unibe.ch (B.E. Kunz)

13

14 **Abstract**

15 During the late Palaeozoic, lithospheric thinning in part of the Alpine realm caused high-temperature low to medium
16 pressure metamorphism and partial melting in the lower crust. Permian metamorphism and magmatism has been
17 extensively recorded and dated in the Central, Eastern and Southern Alps. However, Permian metamorphic ages in the
18 Western Alps so far are constrained by very few and sparsely distributed data. The present study fills this gap. We
19 present U/Pb-ages of metamorphic zircon from several Adria-derived continental units now situated in the Western
20 Alps, defining a range between 286 and 266 Ma. Trace element thermometry yields temperatures of 580–890°C from
21 Ti-in-zircon and 630–850°C from Zr-in-rutile for Permian metamorphic rims. These temperature estimates, together
22 with preserved mineral assemblages (garnet–prismatic sillimanite–biotite–plagioclase–quartz–K-feldspar–rutile), define
23 pervasive upper-amphibolite to granulite facies conditions for Permian metamorphism.

24 U/Pb-ages from this study are similar to Permian ages reported for the Ivrea Zone in the Southern Alps and
25 Austroalpine units in the Central and Eastern Alps. Regional comparison across the former Adriatic and European
26 margin reveals a complex pattern of ages reported from late Palaeozoic magmatic and metamorphic rocks (and relics
27 thereof): two late Variscan age groups (~330 Ma and ~300 Ma) are followed seamlessly by a broad range of Permian
28 ages (300–250 Ma). The former are associated with late-orogenic collapse; in samples from this study these are weakly
29 represented. Clearly dominant is the Permian group, which is related to crustal thinning, hinting to a possible initiation
30 of continental rifting along a passive margin.

31

32 **Keywords:** Permian HT-metamorphism, Western Alps, Adriatic margin, zircon geochronology

33

34 **1. Introduction**

35 Polymetamorphic basement rocks are exposed along the entire Alpine chain (e.g., Schmid et al. 2004; von Raumer
36 2013). Variscan and Permian metamorphic and magmatic rocks are abundant (e.g., Marotta and Spalla 2007; von
37 Raumer 2013; Spalla et al. 2014), though only as relics where Alpine metamorphic overprint is strong. Following the
38 Variscan orogeny, the Alpine realm underwent extension and lithospheric thinning, associated with regional high-
39 temperature (HT) medium/low pressure metamorphism in the lower and mid continental crust, as well as widespread
40 magmatism at all crustal levels. Evidence of metamorphism associated with Permo-Triassic lithospheric thinning is
41 widely documented in the Eastern and Central Alps (e.g., Schuster and Frank 1999; Thöni 1999; Schuster et al. 2001a;
42 Hermann and Rubatto 2003; Gaidies et al. 2008a; Schuster and Stüwe 2008; Thöni and Miller 2009; Galli et al. 2011,
43 2012; Petri 2014). In the Southern Alps, the Ivrea Zone represent a tilted cross section through the lower continental
44 crust of the Adriatic margin (e.g., Mehnert 1975; Fountain 1976; Quick et al. 1995, 2003). The Ivrea Zone is well
45 known for its Permian magmatism (e.g., Rivalenti et al. 1984; Sinigoi et al. 1994; Peressini et al. 2007; Zanetti et al.
46 2013; Klötzli et al. 2014) and HT metamorphism. It exposes a continuous metamorphic field gradient from mid-
47 amphibolite to granulite facies conditions (e.g., Schmid and Wood 1976; Zingg 1980; Sills 1984; Redler et al. 2012;
48 Kunz et al. 2014), and P - T conditions of regional Permian metamorphism are well constrained (e.g., Henk et al. 1997;
49 Luvizotto and Zack 2009; Redler et al. 2012; Ewing et al. 2013). The timing of HT low to medium pressure
50 metamorphism as well as the associated magmatic underplating has been documented by U/Pb zircon and Th-U/Pb
51 monazite age dating (e.g., Vavra et al. 1999; Vavra and Schaltegger 1999; Peressini et al. 2007 and references therein;
52 Ewing et al. 2013). The cooling history has been studied by U/Pb rutile dating (Ewing et al. 2015) as well as Ar/Ar
53 hornblende, K/Ar biotite, and zircon fission-track ages (e.g., Siegesmund et al. 2008). Ewing et al. (2013) showed that
54 U/Pb zircon ages from the Ivrea Zone combined with trace element thermometry (Ti-in-zircon, Zr-in-rutile) provide
55 insight into the T - t evolution during the Permian.

56 Adria-derived slices of continental crust in the Western Alps (Sesia-Dent Blanche nappes and external klippen)
57 also preserve evidence for Permian metamorphism. Especially where Alpine metamorphic overprint is weak, such as in
58 the Seconda Zona Dioritico Kinzigitica (2DK) and Valpelline Series (Fig. 1), pre-Alpine HT assemblages are often
59 visible in the field and have been confirmed in thin sections (e.g., Carraro et al. 1970; Vuichard 1987; Manzotti and
60 Zucali 2013). This led Carraro et al. (1970) to assign the 2DK and Valpelline Series to a single nappe originating from
61 the Ivrea Zone. Where the Alpine HP metamorphic overprint is strong (in internal parts of the Sesia Zone and in
62 external klippen), only local relics of pre-Alpine metamorphism are preserved (e.g., Lardeaux and Spalla 1991). In the

63 Dent Blanche nappe, Permian HT metamorphism has been dated using zircon and monazite between 300–260 Ma (e.g.,
64 Zucali et al. 2011; Manzotti et al. 2012). However, at a regional scale, age data for the Permian HT metamorphic event
65 are lacking so far, whereas Permian magmatism is well documented from gabbroic and granitic intrusives (e.g.,
66 Paquette et al. 1989; Bussy et al. 1998; Rubatto et al. 1999; Monjoie et al. 2007; Cenki-Tok et al. 2011). No temporal
67 relations of the metamorphism in Adria-derived units of the Western Alps have been established so far, nor is it clear
68 what age span the metamorphic imprint across all of the units in the Western Alps may be, or how comparable the
69 duration of the HT low to medium pressure imprint is to the Southern Alps. These space-time relations are relevant to
70 understand the early stages of extension at the Adriatic margin. In the future, the age pattern may serve to constrain the
71 original crustal position of continental fragments now exposed in the Sesia-Dent Blanche nappes and in external klippen
72 units. Therefore we investigated the age and regional distribution of Permian HT metamorphism in the units of the
73 Western Alps that contain Adria-derived lower continental crust.

74 Zircon is an optimal tool for this purpose, as it can preserve robust information on the early evolution of
75 polyphase rocks. In order to relate the zircon U/Pb age data to metamorphic conditions, we used mineral assemblages
76 and relics, the internal textures of zircon, Ti-in-zircon thermometry, and Zr-in-rutile thermometry. Zircon grains
77 typically display complex internal zoning, hence single growth zones were selected for *in situ* U/Pb dating of zircon by
78 LA-ICP-MS. To ensure sufficient amounts of zircon and to simplify comparison within and between datasets, clastic
79 metasediments (mostly metapelites) and leucosomes were analysed. The extent and distribution of Permian
80 metamorphism in continental units from the Western Alps is documented below for 17 select samples from the Sesia
81 Zone (12 from the 2DK, five from the eclogitic micaschist complex), five from the Valpelline Series in the Dent
82 Blanche nappe, and three from the Mt. Emilius Klippe.

83

84 **2. Geological Setting**

85 *Western Alps*

86 The internal Western Alps comprise oceanic and continental units. They result from the large-scale continental collision
87 between two or three continental domains, i.e. Europe, Iberia (Briançonnais), and Adria, (Pfiffner 2009; Handy et al.
88 2010). The oceanic units involved are remnants of the Jurassic to Cretaceous Piemonte-Liguria Ocean. The Sesia-Dent
89 Blanche nappes and the Mt. Emilius Klippe represent continental units derived from the northwest margin of Adria;
90 they mainly comprise slices of Palaeozoic basement rocks that underwent subduction and exhumation since the Upper
91 Cretaceous, hence they were strongly metamorphosed and deformed during Alpine orogeny. Information on their pre-
92 Alpine history is but sporadically preserved. The Sesia-Dent Blanche nappes represent the highest tectonic elements in
93 the Western Alps, thrusting onto the oceanic units. They comprise the Sesia Zone, the Dent Blanche Tectonic System,

94 and the Pillonet Klippe. A comprehensive view of the tectonometamorphic evolution of the Sesia-Dent Blanche nappes
95 was recently published by Manzotti et al. (2014a). The main characteristics of the Sesia-Dent Blanche nappes and the
96 Mt. Emilius Klippe are briefly reviewed here, highlighting the pre-Alpine evolution of these units.

97

98 *Sesia Zone*

99 The Sesia Zone is classically divided into three sub-units: (i) the Eclogitic Micaschist Complex (EMC), (ii) the Seconda
100 Zona Dioritico Kinzigitica (2DK), and (iii) the Gneiss Minuti Complex (GMC) (e.g., Compagnoni et al. 1977), though
101 other subdivisions have been suggested more recently (Babist et al. 2006; Giuntoli and Engi 2016). The EMC and GMC
102 show a strong Alpine metamorphic overprint, whereas the 2DK largely preserves pre-Alpine HT assemblages (e.g.,
103 Carraro et al. 1970; Dal Piaz et al. 1971, 1972; Compagnoni et al. 1977; Gosso 1977; Lardeaux et al. 1982; Vuichard
104 1989; Zucali et al. 2002).

105

106 *Eclogitic Micaschist Complex (EMC)*

107 The EMC is the most internal and biggest unit in the Sesia Zone (Fig. 1). It is mostly made of polymetamorphic
108 basement (mostly metasediments, minor metabasites and metacarbonates) containing derivatives of felsic and mafic
109 intrusives; all rock types show a strong and pervasive Alpine eclogite facies overprint (e.g., Compagnoni et al. 1977;
110 Compagnoni 1977). While the EMC was long regarded as one coherent unit, but recent studies (Regis et al. 2014;
111 Giuntoli and Engi 2016) showed that it comprises several tectonic slices with partly diverging Alpine imprint. From
112 various localities pre-Alpine HT relics (e.g., sillimanite, biotite, garnet, orthoclase) have been reported (e.g., Dal Piaz et
113 al. 1972; Compagnoni 1977; Lardeaux and Spalla 1991; Robyr et al. 2014). Based on such remnants, metamorphic
114 conditions were estimated at 700–800°C and 8–11 kbar for mafic granulites (Lardeaux et al. 1982) and at 700°C and 3.5
115 kbar for sparse amphibolites (Gosso et al. 2010). So far, the age of the pre-Alpine HT metamorphism has not been
116 constrained by radiometric dating. Geochronological studies mostly focused on magmatic rocks, which indicate both
117 Carboniferous (e.g., Ivozio gabbro, 355±9 Ma, Rubatto et al. 1998) and Permian intrusives (Val Sermenza gabbro, 288
118 ±2/-4 Ma, Bussy et al. 1998; Monte Mucrone granitoids, 293 ±1/-2 Ma, Paquette et al. 1989; Bussy et al. 1998; Rubatto
119 et al. 1999; Cenki-Tok et al. 2011).

120

121 *Seconda Zona Dioritico Kinzigitica (2DK)*

122 Rocks of the 2DK mainly surface as discrete bodies in three parts of the Sesia Zone (see Fig. 1). In the northeast (e.g.,
123 Val Mastallone) a coherent body is wedged between the ‘Scisti di Fobello e Rimella’ (Canavese Zone) and the GMC. In
124 more central parts of the Sesia Zone, between Val Sesia and Val del Lys, another fragment of 2DK is situated between

125 the EMC and the GMC. In the area between Val del Lys and Val Ayas, small discontinuous lenses of reddish schists
126 occur (Giuntoli and Engi 2016), which are assigned to the 2DK (Bertolani 1964; Dal Piaz et al. 1971, 2010; Dal Piaz
127 1976; Manzotti et al. 2014a, b). Further to the southwest (Pont Canavese area) small lenses of 2DK outcrops along the
128 contact between the GMC and the EMC. The 2DK unit overall comprise mostly metapelites with minor amphibolites,
129 basic granulites, and metacarbonates (e.g., Carraro et al. 1970). In most of the 2DK bodies the dominant metamorphic
130 imprint is upper amphibolite to granulite facies; however locally, in shear zones and along tectonic boundaries to
131 adjacent units, an imprint at greenschist/blueschist facies conditions can be pervasive (e.g., Vuichard 1987; Ridley
132 1989; Pognante et al. 1988; Stünitz 1989). Pre-Alpine metamorphic conditions in the 2DK have been estimated at 700–
133 830°C and 6–8 kbar (e.g., Vuichard 1987; Pognante et al. 1988). Reliable geochronological constraints on the pre-
134 Alpine history of the 2DK are missing; based on similarities, ages have often been assumed to correspond to those in
135 the Ivrea Zone. Some early studies did date 2DK samples using K/Ar in muscovite (e.g., 177±9 Ma; Hunziker 1974)
136 and Ar/Ar in biotite (e.g., 273–66 Ma; Reddy et al. 1996), but the large range in these results hampers their
137 interpretation.

138

139 *Gneiss Minuti Complex (GMC)*

140 The GMC is the most external sub-unit of the Sesia Zone. Rocks of the GMC are mostly greenschist facies
141 orthogneisses with local occurrence of paragneisses and minor calcsilicates (e.g., Compagnoni et al. 1977). It remains a
142 debate whether the GMC reached HP conditions during Alpine times. Some studies reported jadeite relics (Williams
143 and Compagnoni 1983; Spalla et al. 1991), suggesting a minimum pressure of 12 kbar for the Alpine metamorphism of
144 the GMC, but based on detailed mapping (Giuntoli and Engi 2016) the position of these localities is uncertain, and
145 Alpine maximum pressures were likely lower. Pre-Alpine relics in the GMC are rare, although magmatic allanite, K-
146 feldspar and apatite has been reported for some samples from the GMC (Giuntoli 2016).

147

148 *Pillonet Klippe*

149 The Pillonet Klippe, sitting on top of the Piemonte-Liguria oceanic units, lies midway between the external part of the
150 Sesia Zone (GMC) and the Dent Blanche nappe (e.g., Dal Piaz et al. 2001). The Pillonet Klippe is characterised by fine-
151 grained orthogneiss (Permian metagranitoids), paragneisses (Variscan/Permian), metagabbros (Permian), and Mesozoic
152 metasediments including carbonates (e.g., Dal Piaz and Sacchi 1969; Dal Piaz 1976). The Pillonet Klippe preserves
153 evidence of Alpine blueschist facies metamorphism (glaucofane, phengite; Dal Piaz 1976). Ar/Ar data from mica in
154 paragneiss yield Permian ages of 260–253 Ma, whereas Rb/Sr data indicate 310 Ma (Cortiana et al. 1998). U/Pb zircon
155 ages from a leucocratic dyke yield Variscan magmatic ages of 355±4 Ma and 312±5 Ma, while monazite (Th/Pb age:

156 289±9 Ma) and allanite (Th/Pb age: 266±10 Ma) from the same sample indicate a medium temperature/low pressure
157 metamorphic overprint in the Permian (Grossen 2012).

158

159 *Dent Blanche Tectonic System*

160 The Dent Blanche Tectonic System (Manzotti et al. 2014b) is the most external Adria-derived continental unit in the
161 Western Alps (Fig. 1), surfacing north of the Aosta Ranzola fault, resting on top of remnants of the Piemonte-Liguria
162 Ocean. It comprises the Mont Mary nappe and the Dent Blanche nappe, which are separated by a 25 km long Alpine
163 high-strain zone (the Roisan Cignana Shear Zone, Manzotti et al. 2014b). The Mont Mary nappe and the Dent Blanche
164 nappe consist of slices of continental basement rocks, representing sections of late-Palaeozoic upper crust (the Arolla
165 Series in the Dent Blanche nappe and the Lower Unit in the Mont Mary nappe) and lower crust (the Valpelline Series in
166 the Dent Blanche nappe and the Upper Unit in the Mont Mary nappe; e.g., Manzotti et al. 2014a). Remnants of
167 Mesozoic sedimentary cover are represented by the Mont Dolin Series and the Roisan Zone (Ayrton et al. 1982;
168 Manzotti 2011; Ciarapica et al. 2016). The latter unit is strongly deformed and metamorphosed together with basement
169 rocks along the Roisan Cignana Shear Zone. In the Dent Blanche nappe the Valpelline Series consists of metapelites,
170 metabasites, and metacarbonates with a dominant metamorphic imprint at amphibolite to granulite facies conditions
171 (700–800°C, 7–9 kbar), the pre-Alpine age of which remains poorly constrained (e.g., Diehl et al. 1952; Nicot 1977;
172 Gardien et al. 1994; Zucali et al. 2011; Manzotti and Zucali 2013). The Alpine imprint, mainly under greenschist facies
173 conditions, is weak and only locally developed (De Leo et al. 1987). Kienast and Nicot (1971) described Alpine
174 assemblages with kyanite-chloritoid in metapelite, suggesting conditions of 7–8 kbar and ~525°C for the Alpine
175 evolution. In the Upper Unit of the Mont Mary nappe, Permian metamorphic zircon ages ranging from 294–263 Ma
176 have been reported for metasediments from the Valtournenche area (Manzotti et al. 2012). Similarly, in the Valpelline
177 Series, Permian metamorphism has been dated in zircon from a pegmatite (274±1 Ma; Zucali et al. 2011; Manzotti
178 2012) whereas monazite in a migmatite shows a range from late Carboniferous to early Triassic (304–248 Ma; Zucali et
179 al. 2011; Pesenti et al. 2012). Permian magmatic intrusives are well known in the Dent Blanche Tectonic System,
180 notably from the Collon and Cervino gabbros: 284±1 Ma, ID-TIMS U/Pb zircon crystallisation age (Monjoie et al.
181 2007); 246±8 Ma, K/Ar and 257±6 Ma, Rb/Sr biotite cooling ages (Dal Piaz et al. 1977). Felsic intrusives such as the
182 Arolla granite yield zircon crystallisation ages of 290±2 Ma and of 294.5±6.0 Ma (LA-ICP-MS, Manzotti 2012), in
183 agreement with an ID-TIMS age of 289±2 Ma for Arolla orthogneiss (Bussy et al. 1998).

184

185 *External klippen*

186 Adria-derived continental units form several klippen (Fig.1) situated between sub-units derived from the Piemonte-
187 Liguria Ocean, specifically below the Combin zone and on top of the Zermat-Saas zone (e.g., Dal Piaz 1976, 1999;
188 Ballèvre et al. 1986). The two largest of these outliers are the Mt. Emilius Klippe and the Glacier-Rafray Klippe, both
189 situated south of the Aosta-Ranzola fault. They comprise pre-Alpine basement rocks (metapelites, -basites, -granites,
190 and carbonates) overprinted by Alpine eclogitic metamorphism and locally retrogressed at greenschist facies conditions
191 (e.g., Dal Piaz and Nervo 1971; Dal Piaz et al. 1983). Evidence of pre-Alpine metamorphism in the Mt. Emilius Klippe
192 is preserved as mineral relics (e.g., garnet, rutile, zircon), and P - T conditions for HT metamorphism have been
193 estimated to 700–750°C at maximum pressure of 6–8 kbar (Dal Piaz et al. 1983). The only constraints on the age of pre-
194 Alpine metamorphism for the Mt. Emilius Klippe are based on Rb/Sr whole rock data; these yield ages of ~450 Ma
195 (Hunziker 1974). Granitic intrusives gave early Permian zircon crystallisation ages of 293 ± 3 Ma (Bussy et al. 1998).

196

197 **3. Analytical methods**

198 All sample preparation and analytical work was done at the Institute of Geological Sciences, University Bern. Rock
199 samples were disaggregated using a Selfrag Lab system. Zircon was separated by classical heavy mineral separation,
200 hand picked, mounted in acryl/epoxy and polished to equatorial section. CL-images were made using a ZEISS EVO 50
201 scanning electron microscope. Electron-microprobe analysis on rutile was performed on polished thin sections with a
202 JEOL JXA8200. Measurements for zircon U/Pb-geochronology and trace elements were performed by LA-ICP-MS
203 using a GeoLas-Pro 193 nm ArF Excimer laser system (Lambda Physik) combined with an Elan DRC-e quadrupole
204 mass spectrometer (Perkin Elmer). Detailed analytical protocols are reported in the Online Resource 1. U- and Th-
205 concentrations were measured during geochronological and during trace element analysis, concentrations reported here
206 and discussed are the data obtained during geochronology measurements as they represent the same sample volume as
207 the U/Pb dates. The term date refers to individual $^{206}\text{Pb}/^{238}\text{U}$ spot analyses, while the term age is used for groups of
208 $^{206}\text{Pb}/^{238}\text{U}$ dates that are regarded as geologically significant.

209

210 **4. Sample description**

211 The present study emphasises mineral assemblages and relics associated with Permian HT metamorphism. Other
212 mineral phases not related to HT metamorphism in part reflect post-Permian retrogression or Alpine metamorphism. In
213 some units, such as in the EMC, southwestern parts of the 2DK, and the Mt. Emilius Klippe the Alpine metamorphism
214 was pervasive, and its products can be identified with confidence. However, in the northeastern and central parts of the
215 2DK and in the Valpelline Series the generations often cannot be distinguished unambiguously. Sample localities (Fig.

216 1) and further information (e.g., GPS position, mineral assemblages, main metamorphic imprint) for each sample are
217 given in table 1. Mineral abbreviations follow Kretz (1983) and migmatite terminology Sawyer (2008).

218

219 *Eclogitic Micaschist Complex (EMC)*

220 The samples from the EMC (Fig. 1) are micaschists with a pervasive Alpine eclogite facies imprint; assemblages (table
221 1) comprise white mica (phengite and paragonite), quartz, garnet, epidote, and rare glaucophane and clinozoisite.
222 Accessory phases are allanite, rutile, titanite, graphite, and ilmenite. Sample FG 1347 additionally preserves chloritoid,
223 and sample ROMu-1 has omphacite. Strong Alpine deformation and a HP metamorphic overprint erased most
224 macroscopic evidence of pre-Alpine metamorphism. At the micro-scale, isolated mineral relics remain, notably as cores
225 of garnet porphyroblasts and zircon, very sparsely monazite occurs as well. In none of the micaschist samples we
226 studied is a more complete record of the pre-Alpine metamorphic HT evolution preserved, but coronitic domains in
227 other lithotypes of the EMC have been reported (e.g., Zucali 2011) from some areas.

228

229 *Seconda Zona Dioritico Kinzigitica (2DK)*

230 In the field the samples from most 2DK bodies (Fig. 1) show evidence of pre-Alpine HT metamorphism and partial
231 melting, based on their mineral assemblages, coarse grain size, and separation of leucosome and melanosome domains
232 (see Fig. 2). Near contacts to the EMC or the GMC, the 2DK rocks show an Alpine blueschist to greenschist facies
233 overprint. Permian HT metamorphic assemblages (table 1) include garnet, biotite, sparse sillimanite, plagioclase, K-
234 feldspar, quartz and local rutile. Accessory phases associated with the HT assemblage are mostly zircon, monazite,
235 apatite, ilmenite, and graphite. Retrogression is marked by chlorite replacing biotite and garnet, white mica and
236 epidote/clinozoisite replacing plagioclase, and monazite showing coronas of apatite and allanite. The samples from the
237 SW 2DK additionally contain Alpine glaucophane, albite, and titanite. In sample IIDK 54 biotite shows exsolution of
238 very fine rutile needles, and small, pale green aggregates of chloritoid and amphibole reveal retrogression or a low-
239 grade overprint. Alpine metamorphic overprint increases from absent to minor in the NE 2DK, to a faint greenschist
240 facies overprint in the central 2DK, and a strong greenschist to blueschist facies overprint in the SW 2DK.

241

242 *Valpelline Series*

243 Samples from the Valpelline Series of the Dent Blanche nappe were collected along the Valpelline valley (Fig. 1, table.
244 1). All samples show field evidence indicating HT metamorphism and partial melting, such as a coarse grain size,
245 migmatite textures, distinct leucosome and melanosome domains (Fig. 2). In thin section pre-Alpine HT assemblages
246 including garnet, biotite, plagioclase, K-feldspar, sillimanite, muscovite and quartz are well preserved. Zircon, rutile,

247 monazite, apatite, ilmenite, and graphite are the most common accessory phases associated with the HT assemblage.
248 Manzotti and Zucali (2013) estimated (peak) P - T conditions of $814\pm 40^\circ\text{C}$ and 6–8 kbar for samples VP 66 and VP 74.
249 Sericite, epidote/clinozoisite, and chlorite indicate Alpine retrogression.

250

251 *Mt. Emilius Klippe*

252 The three samples from the Mt. Emilius Klippe are from two localities (see Fig. 1; Tab. 1). The metasediments sampled
253 show reddish weathering and a layered appearance. All three samples show Alpine HP overprint and variable
254 greenschist retrogression. They are dominated by the HP assemblage white mica, garnet, quartz, chlorite, glaucophane,
255 and clinozoisite with accessory titanite, allanite, and rutile. Minerals retaining information about pre-Alpine
256 metamorphism are cores of large garnet porphyroblasts, of dark brown/red rutile grains ($>200\ \mu\text{m}$), and of zircon.

257

258 **5. Zircon**

259 *5.1 Zircon textures*

260 All samples in our study contain zircon, but the quantity, quality (ideally clear, not fractured and non-metamict) and
261 grain size varies from sample to sample. The samples from the EMC show a large variability, some have abundant
262 grains of good quality and grain sizes up to 100–200 μm , while other samples only contain few (<20) grains of poor
263 quality and small grain sizes ($<70\ \mu\text{m}$). The metapelites from the 2DK, Valpelline Series and the Mt. Emilius Klippe
264 usually have sufficient quantities of good quality zircon with grain sizes up to 200 μm . The highest amount of high-
265 quality zircon with grain size up to 500 μm was found in leucosomes from the 2DK and Valpelline Series.
266 Representative CL-images of zircon are shown in Fig. 3. The samples from the EMC mostly have short-prismatic zircon
267 (Fig. 3a–d), while zircon from the 2DK, Valpelline Series and Mt. Emilius Klippe often show roundish shapes (Fig. 3
268 e–s). In some samples (e.g., leucosome) of these units crystals with (short) prismatic habit are also present (Fig. 3i). The
269 internal morphology of zircon crystals varies from sample to sample, even from grain to grain in some samples. Many
270 samples preserve detrital cores, with one or several metamorphic overgrowth zones, while other samples show newly
271 grown Permian metamorphic zircon only. Internal textures within detrital cores are diverse, but oscillatory zoning is the
272 most common type. A first very narrow metamorphic overgrowth usually has a bright CL-emission, a turbulent texture,
273 and many inclusions (Fig. 3e, m); however, such a bright rim is not present (or not preserved) in all grains. The most
274 common type of metamorphic overgrowth has a dark-CL emission with either uniform texture, sector or fir-tree zoning
275 (e.g., 3b–d, e, g–l, o–s). In addition, some migmatite samples from the 2DK, Valpelline Series and Mt. Emilius Klippe
276 commonly show oscillatory zoning (Fig. 3n). A fourth Permian metamorphic overgrowth rim is present in some

277 samples, it shows very bright CL-emission and a mostly uniform texture (Fig. 3 a–d, j, o). Samples from the EMC (FG
278 12157, FG 1315, FG 1347) also show an Alpine metamorphic zircon overgrowth (outermost grey rim in Fig. 3 a, d).

279

280 5.2 U/Pb-geochronology

281 Table 2 gives an overview of the range in Permian and detrital U/Pb zircon dates, uranium and thorium concentration,
282 Th/U ratios, as well as weighted mean ages for each sample. Figure 4 shows probability density plots (PDP) for
283 individual samples, while Fig. 5 shows PDP for the six units. The full data set with individual analyses is given in the
284 Online Resource 6; only concordant $^{206}\text{Pb}/^{238}\text{U}$ dates are reported in all tables. A representative selection of CL-images
285 with location of LA-ICP-MS measurement spots is given in Online Resources 5. Weighed mean ages and unmixing
286 ages have been calculated with Isoplot v4.15 (Ludwig 2003).

287 In the five EMC samples analysed, seventeen detrital cores give a range of dates from 790–415 Ma, and 53
288 metamorphic rims range from 313–222 Ma (Fig. 4a). In samples from the northeastern 2DK 16 zircon cores show a
289 range of dates between 1000–500 Ma, and 106 analyses of metamorphic overgrowth rims yield an overall range
290 between 311–217 Ma (Fig. 4b). In the central 2DK body 16 detrital cores yield a range from 1800–450 Ma, and 63
291 metamorphic overgrowth rims have a range from 329–266 Ma (Fig. 4c). For the 2DK slices in the southwest Sesia
292 Zone, five analyses of detrital cores define a range of dates from 560–352 Ma, 79 dates of metamorphic overgrowth
293 rims range from 305–259 Ma (Fig. 4d). Five samples from the Valpelline Series yield 13 analyses of partially resorbed
294 cores, with dates ranging from 1500–350 Ma; 75 analyses of metamorphic rims range from 330–230 Ma (Fig. 4e). In
295 the samples from the Mt. Emilius Klippe, 19 analyses of detrital cores yield dates from 900–450 Ma, and 29 analyses
296 for metamorphic rims range overall from 327–264 Ma (Fig. 4f).

297 All Permian dates (see Fig. 5) from the EMC combined form a broad peak in the PDP, spanning from 300–280
298 Ma with a maximum at ~285 Ma, giving a weighted mean age (WMA) of 285.9 ± 2.7 Ma ($n=46$; $\text{MSWD}=2.9$). A
299 similar range is observed in the central 2DK (main peak ~286 Ma; WMA: 285.8 ± 1.9 Ma, $n=55$, $\text{MSWD}=2.5$), Mt.
300 Emilius Klippe (main peak ~285 Ma; WMA: 285.7 ± 2.2 Ma, $n=22$, $\text{MSWD}=1.4$) and one of two peaks from the
301 Valpelline Series (~283 Ma; Isoplot unmix age: 283.5 ± 1.7 Ma). The data from the SW 2DK show a broad range of
302 dates with several unresolved peaks in PDP at ~286 Ma, ~280 Ma and ~270 Ma (Isoplot unmix ages: 287.3 ± 1.5 Ma,
303 278.4 ± 2.0 Ma, 268.6 ± 1.8 Ma). The dates from the NE 2DK form a well-defined peak at ~277 Ma (WMA: 277.0 ± 1.1
304 Ma; $n=103$, $\text{MSWD}=1.9$) falling in-between the older peak (286–283 Ma) and the younger peak of the Valpelline
305 Series at ~266 Ma (Isoplot unmix age: 265.6 ± 1.8 Ma). Few dates from the EMC, NE 2DK and Valpelline Series scatter
306 towards younger ages between 260–220 Ma.

307

308 5.3 Zircon trace element geochemistry

309 Thorium and uranium concentration were routinely analysed with the U/Pb data (table 3 and Online Resource 6). For
310 select samples from the 2DK and Valpelline Series trace elements (P, Y, Hf, REE) were separately analysed (Online
311 Resource 6). Th/U ratios of Permian zircon from the EMC and central 2DK (Fig. 5b) are generally low ~ 0.01 – 0.001 ,
312 while high Th/U ratios >0.1 prevail in the NE and SW 2DK. Permian zircon from the Valpelline Series and Mt. Emilius
313 Klippe shows a range of Th/U ratios from 0.01 to >0.1 . In the Valpelline Series there is an apparent trend for higher
314 Th/U ratios with younger ages (Fig. 5b).

315 LREE and MREE patterns of Permian zircon from the 2DK and Valpelline Series broadly overlap for all
316 samples, while HREE patterns show variation within and/or between samples. Two major groups can be distinguished:
317 (i) steep HREE slopes with Gd_N/Lu_N of 3–30 and (ii) flat to slightly negative HREE slopes with Gd_N/Lu_N between 0.4–
318 2. Zircon from leucosome samples (IIDK 52c, IIDK 66 and VR1015) generally fall into the first group of steep HREE
319 pattern and have overall uniform REE pattern within their zircon population. Zircon from metapelitic samples mostly
320 show significant variation in their HREE pattern within each sample (Gd_N/Lu_N 0.4–30), except of sample VR 0909,
321 which has overall flat and uniform HREE patterns (Gd_N/Lu_N 0.62–1.54). Only in one sample (VP 66) from the
322 Valpelline Series a clear correlation of HREE patterns and ages has been found; steep HREE slopes (Gd_N/Lu_N 12–123)
323 are associated with older ages (284–297 Ma), while flat slopes are present in the age generation around 260 Ma. A
324 negative Europium anomaly is present in all Permian zircon (Eu/Eu^* 0.03–0.44).

325

326 5.4 Ti-in-zircon thermometry

327 Titanium concentration in zircon was measured by LA-ICP-MS either simultaneously with U/Pb measurements or as
328 part of trace element measurements (for detailed analytical protocols see Online Resource 1). Temperatures were
329 calculated using the calibration from Watson et al. (2006). Except where stated otherwise, all samples contain rutile and
330 quartz, but in some samples all rutile may be Alpine in age. The data presented are associated with Permian
331 metamorphic zircon rims; an overview for each sample is given in Tab. 3 and Fig. 6; the Online Resource 6 shows
332 individual analyses. Where rutile was absent during zircon growth, the TiO_2 -activity was reduced, and temperatures
333 represent minimum values. Ti-in-zircon concentrations range from a few ppm in the central 2DK (1–4 ppm) and EMC
334 (2–3 ppm), to 5–15 ppm in most samples of the NE and SW 2DK, Valpelline Series, and Mt. Emilius Klippe. Three
335 samples (IIDK 17, VR 0909 and EM1-1056) show very high concentration (>25 ppm). In most samples from the EMC
336 and one from the Mt. Emilius Klippe (EM1-1051), growth zones are narrow, requiring a small spot for LA-ICP-MS
337 analysis. As Ti-concentration in these samples was low, they were below detection limit (<3 ppm). For the EMC (FG
338 1249) Ti-concentrations could be measured only in one sample. Due to the strong Alpine metamorphic overprint in

339 EMC samples it is not possible to be sure whether rutile and/or ilmenite were part of the HT assemblage, hence the Ti-
340 in-zircon concentration (2–3 ppm) and temperatures (618–641°C) derived from FG 1249 are minimum values. Except
341 for a few outliers, Permian zircon from the NE 2DK shows high (4.3–15.1 ppm) Ti concentrations. In all samples from
342 that unit rutile is present and considered part of the HT assemblage; the data translate to Ti-in-zircon temperatures of
343 ~680–780°C for Permian growth. In the central 2DK, all measured Ti-in-zircon concentrations for Permian zircon rims
344 are low (<5 ppm except for one outlier). In these samples, rutile was found only as exsolution needles in biotite. Due to
345 the notable greenschist facies overprint we are unsure if rutile was present during Permian HT metamorphism. The
346 ~580–680°C obtained for the central 2DK are thus considered minimum temperatures for the Permian metamorphism.
347 The samples from the southwestern 2DK show two contrasting ranges, VS 1009 and VS 1015 have low to intermediate
348 Ti-concentrations (2.3–7.8 ppm) in their Permian zircon growth zones. On the other hand, sample VR 0909 retains very
349 high Ti-concentrations (~20–40 ppm). Despite a relatively strong greenschist to blueschist facies overprint, rutile can be
350 found, and we consider it part of the HT assemblage in the samples from the SW 2DK. Based on this, the distinct Ti-in-
351 zircon concentrations are thought to represent real differences in temperature (~627–888°C) during Permian zircon
352 growth. Ti-concentrations increase from low (3.8–7.8 ppm) in sample VP 1402 towards higher values (2.6–13.5 and
353 4.1–10.0 ppm) in samples VP 66 and VP 74. In all samples from the Valpelline Series, rutile is present, and Ti-in-zircon
354 temperatures ranging from 642–768°C are likely to represent zircon growth during Permian HT metamorphism. In two
355 samples from the Mt. Emilius Klippe, for which Ti-in-zircon data could be acquired, Ti-concentrations similarly
356 dispersed as in the samples from the SW 2DK, ranging from 4.8–10.6 ppm in sample EM1-1049, and 11.5–25.9 ppm in
357 sample EM1-1056. Despite a strong Alpine metamorphic overprint in the samples from the Mt. Emilius Klippe,
358 evidence for rutile belonging to the HT assemblage is present, and Ti-in-zircon temperatures of 680–832°C are
359 indicated for Permian zircon growth.

360

361 **6. Zr-in-rutile thermometry**

362 Zr-in-rutile concentrations were measured by electron microprobe; for detailed analytical conditions and protocols see
363 supplementary material Online Resource 1. Rutile is present in many samples, but fresh HT rutile was found only in a
364 few samples that allowed Zr-in-rutile measurements for the calculation of temperatures to be warranted. The range of
365 Zr-concentration and temperatures, calculated using the Watson et al. (2006) calibration, are listed in Tab. 3 and plotted
366 in Fig. 7. Individual analyses for the six measured samples together with a selection of BSE images from the analysed
367 rutile grains are given in Online Resource 5 and 6.

368 In HT assemblages rutile is commonly dark red to brown, and crystals are up to 700 µm in diameter. In the samples
369 from the EMC no large, dark HT rutile grains could be found. Instead, rutile in these samples is small (10–150 µm) and

370 usually of light brown to yellow colour. Zr-concentrations were measured in one sample from the EMC (FG 1249) to
371 test if rutile Zr-contents were reset during Alpine-HP overprint. Indeed, Zr-concentrations in this sample range from 4–
372 288 ppm, corresponding to temperatures of 385–639°C, clearly cooler than the Permian metamorphism in the 2DK and
373 Valpelline Series. In the northeastern 2DK, rutile is very common, but occasionally replaced in part by ilmenite and/or
374 titanite and/or showing exsolution of μm -sized zircon/baddeleyite needles. Fresh rutile was found in sample IIDK 54.
375 Avoiding areas showing replacement or exsolution, the sample yields Zr-concentrations of 563–2186 ppm,
376 corresponding to temperatures of \sim 690–840°C. In samples from the central 2DK lens, no HT rutile was found.
377 Occasionally very fine rutile needles occur in exsolution textures in HT biotite. Owing to the strong greenschist facies
378 overprint in the southwestern 2DK, fresh rutile is rare, but in sample VR 0909 some rutile grains were unaffected by
379 ilmenite and/or titanite replacement. These have a range in Zr-concentration of 571–2035 ppm, i.e. a temperature range
380 of \sim 700–830°C, similar to the northeastern 2DK. Samples from the Valpelline Series commonly show abundant fresh
381 HT rutile. Two samples (VP 66 and VP 74) were selected for Zr-measurements. Both datasets show a slightly larger
382 spread than in the 2DK samples, with Zr-concentrations of 400–2395 ppm (\sim 665–850°C) for sample VP 66 and 346–
383 2049 ppm (\sim 630–830°C) for VP 74. For samples from the Mt. Emilius Klippe, despite strong Alpine overprint, some
384 pre-Alpine rutile grains are preserved. Sample EM1-1051 shows dark brown rutile grains, locally overgrown or rimmed
385 by fine-grained, lighter coloured rutile grains, and small, separate light brown to yellow rutile is also found. Rutile
386 grains of all sizes and colours were analysed for Zr-concentrations resulting in a range from 10–1190 ppm (432–
387 770°C). The lowest Zr-concentrations were found in the rims of some grains, while the highest usually were found in
388 the centre. However some low values were from inside dark-brown rutile grains, indicating reset Zr-concentrations in
389 rutile without textural/microscopic evidence. For the Mt. Emilius Klippe samples the calculated Zr-in-rutile
390 temperatures ranging from \sim 620–770°C are thought to reflect Permian HT metamorphism; the results overlap closely
391 with those for the 2DK and Valpelline Series. Temperatures ranging from 430–600°C are similar to those inferred to
392 represent Alpine temperatures in the sample from the EMC (Fig. 7b). The diversity of the Zr concentration in rutile
393 from the Mt. Emilius Klippe indicates several generations of rutile growth and partial resetting of Zr in HT-rutile.

394

395 **7. Discussion**

396 In the Alps, HT metamorphism has long been related to the late Variscan orogenic evolution (e.g., Scherrod 1988;
397 Desmons et al. 1999 and references therein; Frisch and Neubauer 1989; Neubauer et al. 1989; Gardien et al. 1994) and
398 associated with thermal relaxation in the over-thickened lithosphere and late orogenic collapse. Owing to Alpine
399 overprint, the age of this metamorphism is largely assumed to be coeval to the magmatic evolution, which mostly spans
400 a range from 340–295 Ma (e.g., Bussy et al. 2000; Online Resource 4). Over the past two decades studies in late

401 Palaeozoic metamorphic rocks increasingly recognised a distinct Permian thermal phase, which has been variably
402 associated with upwelling of the asthenospheric mantle, mafic underplating, and continental rifting (e.g., Diella et al.
403 1992; Bertotti et al. 1993; Müntener and Hermann 2001; Marotta and Spalla 2007; Schuster and Stüwe 2008). For the
404 Eastern Alps, crustal-scale extensional processes in the course of the separation of Europe and Adria are now thought to
405 be responsible for the LP-HT Permian metamorphism (e.g., Schuster et al. 2001a). A similar Permian extensional
406 evolution, characterised by a high thermal regime, has been proposed also for the Western Alps (e.g., Lardeaux and
407 Spalla 1991; Marotta and Spalla 2007; Schuster and Stüwe 2008; Beltrando et al. 2007), but such a separate Permian
408 evolution was so far supported mostly by geochronological data from magmatic rocks (i.e. Permian gabbros and
409 granitoids; e.g., Paquette et al. 1989; Bussy et al. 1998; Bussy and Cadoppi 1996; Rubatto et al. 1999; Bertrand et al.
410 2005; Monjoie et al. 2007; Cenki-Tok et al. 2011); overall, these indicate an age group (mostly 290–270; Fig. 9; Online
411 Resource 3) distinct from the late-Variscan one. A HT metamorphic imprint of Permian age has long been assumed, but
412 geochronological data to support this idea have been few and far between (e.g., Zucali et al. 2011; Manzotti, 2012;
413 Pesenti et al. 2012). The present study fills this gap by adding age data of Permian metamorphic rocks from the Western
414 Alps, in particular from Adria-derived tectonic units. The overall age range spans a time interval of 40–50 Myr in the
415 Permian, indicating that HT metamorphism in the continental crust was protracted and indeed defines a separate group
416 than the late-orogenic Variscan one.

417

418 *Zircon U/Pb age interpretation*

419 Zircon grains dated in this study were separated from metasediments, mostly metapelites, i.e. from samples that are
420 expected to have behaved similarly under comparable metamorphic conditions. Additionally garnet-bearing leucosome
421 veins or dykes were selected from some units (2DK and Valpelline Series). In many samples zircon shows crystal-
422 habits ('soccer-ball' shaped; Fig. 3g, h, k, o, r, s; c.f. Vavra et al. 1996, 1999) and internal textures that indicate growth
423 at HT metamorphic conditions (dark-CL, uniform, sector or fir-tree zoning; Fig. 3c, f, h, i, j, s) or in anatexis
424 environments (oscillatory zoning; Fig. 3l, n, r) (e.g., Harley et al. 2007). Analytical spots for dating of metamorphic
425 growth of zircon were chosen based on such textural criteria.

426 To discuss the spatial-temporal evolution regionally, it is useful to distinguish two sample domains: Domain A
427 comprises the EMC, central 2DK, and Mt. Emilius Klippe; domain B includes the NE 2DK, SW 2DK, and the
428 Valpelline Series.

429 U/Pb zircon dates ranging from ~310 to 260 Ma are found all over domain A and B, attesting the regional
430 extent of late Palaeozoic HT metamorphism in the Adria-derived units (shown in Figure 9, discussed below). The data
431 presented in the PDP of Fig. 4 and 5 show that the overall distribution of dates is scattered among samples and units;

432 however, Fig. 5 shows that pooling of ages allows us to distinguish between age groups among the units. Two main age
433 groups of metamorphic zircon growth are distinguished in both domains (Fig. 5a): the first one (~290–280 Ma) is
434 coeval with or only slightly younger than the Permian magmatism (~294 and ~284 Ma) reported for the Western Alps;
435 the second group (~277–266 Ma) is clearly younger.

436 In domain A the first age group dominates the zircon population (Fig. 5a), it has a weighted mean age of 286 ± 2
437 Ma. In the EMC and central 2DK this age group is generally associated with low Th/U ratios (Fig. 5b) and low Ti-in-
438 zircon concentration (Fig. 6b), but no such trend is evident in the data from the Mt. Emilius Klippe. In many samples
439 from these three areas Permian metamorphic overgrowths are narrow, and detrital cores dominate the zircon grains (Fig.
440 3). Textures indicate limited zircon dissolution and minor new growth during HT metamorphism, possibly because
441 fluid/melt supply was limited or the heat pulse short-lived, thus not allowing a large quantity of zircon to dissolve or
442 grow during the Permian.

443 In domain B the first age group is also present (SW 2DK: 287 ± 2 Ma, Valpelline Series: 283 ± 2 Ma; Fig. 4, 5a),
444 but it is the second age group (~277–266 Ma) that dominates the zircon population. The first age group in domain B
445 lacks the characteristics of low Th/U and Ti-concentration (Fig. 5b, 6b) and growth zones are wider than in domain A.
446 Whereas a distinct peak is found in the PDP for the NE 2DK, with a weighted mean age of 277 ± 1 Ma (Fig. 5a), no clear
447 age peak emerges for the SW 2DK (Fig. 4d, 5a), just a range of ages that may comprise unresolved peaks. Using
448 Isoplot's unmixing age function, three age generations emerge at 287 ± 2 Ma, 278 ± 2 Ma and 268 ± 2 Ma that do
449 correspond to the peaks discernible in the PDP. The Valpelline Series shows a bimodal age distribution with two
450 incompletely separated peaks (Fig. 5a). The Isoplot unmixing age function yields an age at 283 ± 2 Ma and a younger
451 generation at 266 ± 2 Ma. The results indicate that the NE and SW 2DK and Valpelline Series experienced a first zircon
452 growth phase as well as a second one some ~10–20 Myr later. In domain B metamorphic overgrowth dominates most of
453 the zircon grains, whereas core remnants dominates in Domain A. In domain B HT conditions evidently lead to more
454 resorption either because of higher metamorphic conditions and/or longer duration of these conditions. Extensive partial
455 melting, visible as migmatites, lead to significant zircon resorption followed by new growth over ~20 Myr. Samples in
456 all of domain B show HT metamorphic assemblages, high Th/U ratios in zircon (0.01–0.8; Fig. 5b), and zircon textures
457 indicating growth at amphibolite to granulite facies conditions (Fig. 3f; fir-tree and sector zoning; c.f., Vavra et al.
458 1996, 1999). Attempts to discriminate different growth phases based on (H)REE patterns (e.g., Rubatto 2002) were
459 inconclusive: HREE slopes vary significantly between steep and flat among and within samples, and no correlation to
460 age, Th/U ratios, Ti-in-zircon temperatures or textures is evident. This may indicate local processes in small-scale
461 domains, such are expected if partial melts migrate through compositionally heterogeneous rocks.

462 Age differences are evident also among individual samples. Migmatite parts sampled in close proximity, both
463 in the 2DK (e.g., melanosome IIDK 65; leucosome IIDK 66) and Valpelline Series (melanosome VP 1403a; leucosome
464 VP 1403b) show differences in their age distribution (Fig. 4c and 4e). Compared to melanosomes, leucosomes tend
465 towards older ages indicating that bulk rock chemistry and/or melt depletion have an influence on apparent ages. Yet, in
466 other studies (e.g., Rubatto et al. 2001) the age difference between leucosome and melanosome was inverse, the
467 leucosome being slightly younger than the melanosome. Yakymchuk and Brown (2014) concluded that apparent age
468 differences between individual samples are most likely caused where migmatites reach the solidus at different
469 temperatures because of differences in local bulk rock composition and/or melt depletion.

470 Zircon in domain A are characterised by an age of 286 ± 2 Ma, generally low Th/U ratios, low Ti concentration
471 and narrow Permian metamorphic growth zones. In contrast zircon of domain B shows two age groups (~ 287 – 283 Ma
472 and ~ 277 – 266 Ma), with high Th/U ratios in zircon, high Ti concentration and wide Permian metamorphic overgrowths
473 rims. The reasons for these differences cannot unambiguously be identified. A possibility is that domain A and B
474 experienced different duration and intensity of partial melting during HT metamorphism. Therefore in domain B more
475 pre-existing zircon has been dissolved and subsequent wider metamorphic rims grew. The varying width of Permian
476 metamorphic growth zones could also explain the difference in age pattern we observed. Due to the spot size during
477 LA-ICP-MS measurements 32 – 16 μm we bias our results towards growth zones at least slightly wider than our spot
478 size. Therefore the absence or limited number of dates between 277 – 266 Ma in domain A might not imply that they do
479 not exist, they simply could not be measured.

480 Scattered younger ages (<260 Ma) are associated with zircon internal textures that indicate late stage fluid-
481 assisted recrystallisation (Fig. 3a, d, o; c.f. SCA, Vavra et al. 1999). Such textures occur in both domains; most
482 abundantly they are observed in EMC samples (Fig. 5a), but they are locally present in samples from the NE 2DK and
483 Valpelline Series as well. The age of such recrystallisation events is difficult to specify: they may immediately follow
484 the Permian HT metamorphism or at a later time, perhaps in the Alpine cycle.

485
486 *Significance and interpretation of zircon and rutile trace element thermometry*

487 In our study the temperature ranges from both thermometers are similar (~ 600 – 800°C , Fig. 6, table 3 and 750 – 850°C ,
488 Fig. 7, table 3). The lowest Ti-in-zircon temperatures (600 – 650°C) are considered minimum values, as rutile is lacking
489 in some samples and TiO_2 activity may have been reduced (e.g., Watson et al. 2006). On the other hand, the high
490 temperatures (>750 – 800°C) in sample IIDK 17, VR 0909 and EM1-1056 may reflect local heat anomalies, possibly
491 caused by proximal heat sources such as mafic dykes or intrusive stocks. BSE-images of some rutile grains from the
492 EMC, 2DK, and Mt. Emilius Klippe do show exsolution of zircon/baddeleyite needles, but not in samples from the

493 Valpelline Series. Nevertheless Zr-in-rutile temperatures from the 2DK (690–840°C) overlap with those from the
494 Valpelline Series (630–850°C), so Zr-in-rutile temperatures appear not to be reset. For the EMC and Mt. Emilius Klippe
495 clearly lower Zr-in-rutile temperatures (385–639°C and 432–770°C) were measured, and these appear to reflect
496 retrogression.

497 While Ti-in-zircon temperatures in HT rocks commonly are found to be below peak temperatures and may
498 indicate zircon growth during cooling (e.g., Roberts and Finger 1997; Baldwin et al. 2007; Harley 2008) Zr-in-rutile
499 temperatures are interpreted to record metamorphic peak temperatures (e.g., Ewing et al. 2013). Zr-in-rutile
500 temperatures from this study therefore suggests that metamorphic peak temperatures did not exceed 800–850°C in
501 Adria-derived units. The results from trace element thermometry are in good agreement with the P – T data from
502 previous studies, ranging from ~700–800°C at ~6–9 kbar (e.g., Nicot 1977; Lardeaux 1981; Lardeaux et al. 1982; Dal
503 Piaz et al. 1983; Vuichard 1987; Pognante et al. 1988; Lardeaux and Spalla 1991; Gardien et al. 1994; Manzotti and
504 Zucali 2013).

505

506 *Permian metamorphic ages in the Alps*

507 So far few geochronological studies focused on unravelling the age of the HT metamorphism in Adria-derived units of
508 the Western Alps. Recent studies in the Valpelline Series provided a Permian U/Pb zircon age from a pegmatite dyke
509 (274±1 Ma; Zucali et al. 2011; Manzotti 2012) and chemical (EMPA) monazite ages from migmatites (304–248 Ma;
510 Zucali et al. 2011 and 290±4 Ma; Pesenti et al. 2012). In addition, Manzotti et al. (2012) obtained metamorphic U/Pb
511 zircon ages, ranging from 294–263 Ma, for a meta-chert from the Upper Unit in the Mont Mary nappe. These sparse age
512 data indicated a prolonged Permian HT metamorphism for the lower crustal units of the Dent Blanche nappe. The new
513 results presented here affirm the Permian age of HT metamorphism in that unit and document comparable ages in the
514 other Adria-derived lower crustal units studied, i.e. the EMC, 2DK, and Mt. Emilius Klippe. Furthermore, the dataset as
515 a whole clearly indicates that zircon growth occurred in two distinct time intervals of the protracted HT history of these
516 units. The first age group (290–280 Ma) is contemporaneous with the several known, magmatic ages from the Sesia-
517 Dent Blanche nappes (~294 and ~284 Ma; e.g., Val Sermenza gabbro, Collon and Cervino gabbros, Monte Mucrone
518 granitoids, and Arolla granitoid; e.g., Paquette et al. 1989; Bussy et al. 1998; Rubatto et al. 1999; Monjoie et al. 2007;
519 Cenko-Tok et al. 2011; Manzotti 2012). The second age group clearly postdates that intrusive phase by some 10–20 Myr
520 (see Fig. 8). Three questions emerge:

521 (1) How do the Permian ages from our study compare to those from other parts of the Alps?

522 (2) Are two age groups visible also in other regions?

523 (3) What caused the two phases of zircon growth?

524 The 2DK and Valpelline Series are thought to be closely related to the Ivrea Zone (e.g., Carraro et al. 1970),
525 hence we start our comparison with the well documented Permian metamorphism in the Kinzigite Formation of the
526 Ivrea Zone. The Ivrea Zone in the Southern Alps is famous for its cross section through the Permian lower continental
527 crust, displaying a continuous metamorphic field gradient from amphibolite to granulite facies (Kinzigite Formation) as
528 well as mafic underplating (Mafic Complex). Several studies (e.g., Vavra et al. 1999; Peressini et al. 2007; Ewing et al.
529 2013) show that the main age range of metamorphism is ~316–260 Ma. Ewing et al. (2013) found three generations of
530 U/Pb zircon ages at 316 ± 3 Ma, 276 ± 4 Ma and 258 ± 3 Ma within a granulite facies sample from the Kinzigite Formation.
531 Magmatic ages in the Ivrea Zone show a bimodal age distribution. In the ‘central’ Ivrea Zone (Val Sesia) the magmatic
532 activity ranges between ~295–280 Ma, with the main intrusive phase at 288 ± 4 Ma (e.g., Peressini et al. 2007; Sinigoi et
533 al. 2011; Klötzli et al. 2014). In the northeastern part of the Ivrea zone (Finero area), magmatic activity was reported at
534 232 ± 3 Ma (gabbros; Zanetti et al. 2013) and between 212 and 190 Ma (pegmatites; Schaltegger et al. 2015). Our
535 samples from Adria-derived units show little evidence of the oldest age generation found in the Ivrea Zone (316 ± 3 Ma),
536 though some scattered ages >300 Ma are present in all units we have studied. Our first, well-defined age group (286–
537 283 Ma) is only present as a partially resolved age peak (~285 Ma) in the Ivrea Zone (Ewing et al. 2013). The
538 intermediate Ivrea age of 276 ± 4 Ma overlaps with our second age group (277–266 Ma) that dominates in the 2DK and
539 Valpelline Series from the present study (Fig. 8). The youngest metamorphic growth generation (258 ± 3 Ma) in the
540 Kinzigite Formation is only slightly younger than our second age peak in the Valpelline Series (266 ± 2 Ma) (Fig. 5, 8).
541 Metamorphic zircon ages younger than 240 Ma in the Ivrea Zone are usually associated with late stage fluid alteration
542 (e.g., Vavra et al. 1996, 1999), similar to what we infer for our scattered ages <260 Ma in the EMC, Valpelline Series,
543 and NE 2DK. We conclude, based on the U/Pb zircon age groups, mineral assemblages, and metamorphic conditions a
544 similar origin of the Adria-derived units and the Kinzigite Formation of the Ivrea Zone is indeed very likely. The cause
545 of the amphibolite to granulite facies metamorphism and the age of metamorphism have long been debated for the Ivrea
546 Zone. Early studies postulated that the metamorphism was caused by the intrusion of the Mafic Complex (e.g., Sinigoi
547 et al. 1991; Henk et al. 1997), but several more recent studies (e.g., Barboza et al. 1999; Barboza and Berganz 2000;
548 Redler et al. 2012) concluded that these intrusion most likely was not responsible for the regional metamorphism in the
549 Ivrea Zone. The controversy about cause of the age pattern observed in the Ivrea Zone remains as the first phase pre-
550 dates the mafic intrusion by several millions years, and the most abundant age group (~276 Ma) as well as the ~258 Ma
551 ages post-date the intrusion by 10–30 Myr. Similar observations apply in the Malenco unit, a more easterly slice of
552 Adriatic lower continental crust (Fig. 9); Hermann and Rubatto (2003) concluded that the first of three age generations
553 (281 ± 2 Ma) may have been caused by the intrusion of gabbros (281 ± 19 Ma), while subsequent age generations,
554 especially the volumetrically prominent growth generation at 269 ± 3 Ma, required additional heat input, most likely

555 related to lithospheric thinning. The age pattern and observation of age generations clearly postdating the gabbroic
556 intrusions in the Malenco case are similar to what is observed in the Ivrea Zone and, in the present study, in Adria-
557 derived units.

558 Figure 9 shows a tectonic overview map of the Alps with ages and P - T conditions from rocks that experienced
559 Permian HT metamorphism. In addition to the Western Alps, Ivrea Zone, and Malenco unit, notable occurrences in the
560 Austroalpine units of the Eastern Alps are shown, where Permian metamorphism has been recognised with an overall
561 age range of ~290–240 Ma. As in the Ivrea Zone (Vavra et al. 1999; Ewing et al. 2013), the Malenco unit (Hermann
562 and Rubatto 2003) and the Adria-derived units (this study), several growth phases have been established on monazite
563 and detailed Sm/Nd garnet geochronology in the Austroalpine units (e.g., Schuster and Frank 1999; Habler and Thöni
564 2001; Schuster et al. 2001a, b; Gaidies et al. 2008a, b; Thöni et al. 2008; Thöni and Miller 2009; Schuster et al. 2015).
565 Across the Alpine chain some units show a broad range of ages (e.g., Valpelline Series, Ivrea Zone, Monte Rosa nappe,
566 Gruf complex, Malenco unit, Rappold complex, Strallegg complex and Saualpe/Koralpe complex), while other units
567 only show ages from ~290–280 Ma (e.g., EMC, Mt. Emilius Klippe, Campo unit), or only ages <280 Ma (e.g., Matsch
568 unit, Wölz Complex, Plankogel Complex, Jenig Complex, Strieden Complex and Deferegger Complex). Some
569 Austroalpine units furthest to the east and southeast (Fig. 9) show ages generally younger than 275 Ma, indicating a
570 slight trend towards younger ages from west to east (Fig. 8). As stated above the absence of a particular age group in a
571 unit does not imply complete absence of it, possibly age groups could get obscured due to few data (unclear
572 significance) or bias during measurements (e.g., analytical resolution, spot size).

573 In figure 9 Permian magmatic ages within the range of ~300–240 Ma are seen to scatter across the Alpine
574 chain. U/Pb zircon ages for felsic and mafic plutons have a median age of 280 Ma and 285 Ma respectively (Fig. 9;
575 corresponding references in Online Resources 3), while Sm/Nd mineral isochron ages in the Eastern Alps and the Ivrea
576 Zone have a median of ~250 Ma (e.g., Miller and Thöni 1997; Mayer et al 2000; Miller et al. 2011). U/Pb zircon ages
577 from mafic plutons (visible at the present level of erosion) in the Adria-derived units of the Western Alps are
578 dominantly in the age range of 295–285 Ma. The data presented in this study showed that in the Western Alps a
579 metamorphic age group (290–280 Ma) is essentially coeval with these magmatic ages (Fig. 8), yet in several units
580 (Valpelline Series, NE and SW 2DK) a second age group (277–266 Ma) dominates the zircon population (Fig. 8). The
581 fact that abundant and voluminous zircon growth phases as well as detailed Sm/Nd garnet geochronology (Fig. 8) give
582 clearly younger metamorphic ages than the U/Pb zircon intrusion ages do not support to the often-proposed causal
583 connection, i.e. gabbroic intrusions providing the heat for Permian HT metamorphism in the lower and middle crust of
584 the Adriatic margin.

585 Several places in the Alps (e.g., Sesia Zone, Ivrea Zone, Malenco unit or Campo unit; Fig. 9) allow a closer
586 look at the relationship between Permian mafic bodies and Permian metamorphic ages. The EMC in the Sesia Zone
587 hosts several mafic intrusions that were dated to 288 Ma and 285 Ma, the metamorphic ages obtained in this study for
588 the EMC have an average age of 286 ± 2 Ma, this observation support the theory that gabbroic intrusions provided the
589 heat for Permian HT metamorphism. Similar conclusions have been made by Petri (2014) in the Campo unit, where the
590 intrusion of the Sondalo gabbros (289–285 Ma) caused the 288 Ma metamorphism in the surrounding rocks. However
591 in the Ivrea Zone as well as in the Malenco unit the mafic intrusions are dated to 288 Ma (Peressini et al. 2007) and 281
592 Ma (Hansmann et al. 2001) respectively, while metamorphic ages contemporaneous with the intrusion age occur,
593 several phases of voluminous and zircon growth up to 20 Myr younger are reported for both units (e.g., Vavra et al.
594 1999; Hermann and Rubatto 2003; Ewing et al. 2013). Magmatic underplating, pooling of mafic melt at or below the
595 Moho, caused by lithospheric thinning and asthenospheric upwelling have been suggested (Henk et al. 1997) to cause
596 regional scale HT metamorphism. This scenario accounts for regional protracted heating, affecting all crustal levels
597 independent of the local occurrence of Permian intrusions. We regard these intrusions are an effect of magmatic
598 underplating, as well as the HT metamorphism. In areas where magma intruded the shallower (cooler) crustal levels
599 local contact metamorphism is evident (e.g., in the Campo unit), while at deeper crustal levels (e.g., in the Ivrea Zone)
600 thermal effects around intrusive bodies are less well defined, and contact aureoles are hardly distinguishable, due to
601 ambient temperatures being near magmatic temperatures at the time of the intrusion.

602 The Permian evolution is well represented also in the sedimentary record: early Permian strike-slip tectonics
603 resulted in the opening of asymmetric graben basins in the central part of the South-Alpine unit (e.g., Orobic Basin,
604 Collio Basin; Matte 1986; Massari 1988; Cassinis et al. 1995), with dominantly continental deposits and sparse marine
605 deposits (Bellerophon Formation and Pontebba Supergroup; Bosellini 1991). In summary, the Permian evolution is
606 widely recorded in the Alpine realm, with clear structural, magmatic, metamorphic and sedimentary signatures,
607 indicating a temporal link between extensional tectonics, the accumulation of mantle melt at the base of the crust (e.g.,
608 Malenco unit, Müntener and Hermann 1996; Müntener et al. 2000; Ivrea Zone, Voshage et al. 1990), partial melting in
609 the lower crust (e.g., Ivrea Zone, Redler et al. 2012), intrusion of granitic bodies at higher levels (e.g., Arolla Series,
610 Bussy et al. 1998; Serie dei Laghi, Köppel 1974; Schaltegger and Brack 2007) and explosive acid volcanism at the
611 surface (e.g., Serie dei Laghi, Quick et al. 2009). Although there is a clear temporal link between mafic magmatism and
612 HT metamorphism, the regional scale of the Permian thermal effects – documented over more than 600 km from the
613 Western to the Eastern Alps and further east into the basement of the Pannonian basin (Lelkes-Felvári et al. 2003) –
614 indicates that the heat-source for HT metamorphism was not solely provided by mafic melts intruding the crust, but
615 sustained by the upwelling mantle itself.

616

617 **8. Conclusions and Outlook**

- 618 • This study shows that the Permian thermal evolution is preserved in the Adria-derived units of the Western
619 Alps (EMC, 2DK, Valpelline Series, and Mt. Emilius Klippe), with U/Pb zircon ages ranging from 286–266
620 Ma. Mineral assemblages, trace element thermometry, and zircon growth textures indicate amphibolite to
621 granulite facies conditions (~650–850°C) and associated partial melting.
- 622 • Two different domains could be identified based on their ages. Domain A (EMC, central 2DK and Mt. Emilius
623 Klippe) show an age of 286 ± 2 Ma, while domain B (NE and SW 2DK and Valpelline Series) shows a bimodal
624 age distribution of 287–283 Ma and 277–266 Ma.
- 625 • The new dataset confirms the close similarities between the Valpelline Series, the 2DK, and the Ivrea Zone, as
626 already noted by Carraro et al. (1970) on the basis of metamorphic assemblages. Combined with the previous
627 data our results indicate contemporaneous HT metamorphism (over 40 Ma) and magmatism in the lower and
628 middle Permian continental crust forming the Adria derived units of the Alps today.. The HT metamorphism
629 and magmatism are the result of the extensional tectonics and high thermal regime that affected the Adriatic
630 plate at Permian time.
- 631 • The Variscan evolution in Adria-derived units in the Western Alps still remains to be reassessed. Pervasive
632 Permian or Alpine metamorphic overprint may have obliterated much of the Variscan imprint. Especially in lower
633 crustal units, prolonged Permian heating most likely erased evidence from the Variscan metamorphic cycle. Zircon
634 geochronology and thermometry might be also useful in elucidating the Variscan remnants in these units.

635

636

637 **Acknowledgements**

638 We thank Thomas Pettke and Afifé El Korh for assistance with LA-ICP-MS work, Martin Robyr for help with EMPA
639 analysis, and Marco Burn and Roland Oberhänsli for providing sample material from the EMC and Mt. Emilius Klippe.
640 Samples VP 74 and VP 66 were collected during Paola Manzotti's MSc thesis supervised by Michele Zucali. Niklaus
641 Grossen, Remo Widmer, Matthias Bächli, and Rahel Baumann helped with mineral separation, Daniela Rubatto and
642 Bénédicte Cenki-Tok with discussions that helped us improve earlier versions of the manuscript. Ralf Schuster and
643 Geoffroy Mohn are thanked for their constructive reviews. We thank Wolf-Christian Dullo for editorial handling. The
644 Swiss National Science Foundation provided funding (Project 200020-146175).

645

646 **Author contributions**

647 Sample material has been collected/provided by B.E. Kunz, P.M., B.vN., M.B. and F.G.; Geochronological and
648 geochemical data have analysed and by B.E Kunz, P.M. and B.vN.; J.R.D. and P.L. provided assistance and discussion
649 with LA-ICP-MS analysis; B.E. Kunz, P.M. and M.E. wrote the paper.

650

651 **References**

- 652 Ayrton S, Bugnon C, Haarpainter T, Weidmann M, Frank E (1982) Géologie du front de la nappe de la Dent-Blanche
653 dans la région des Monts-Dolins, Valais. *Eclogae Geologicae Helvetiae* 75:269–286
- 654 Babist J, Handy MR, Konrad-Schmolke M, Hammerschmidt K (2006) Precollisional, multistage exhumation of
655 subducted continental crust: The Sesia Zone, western Alps. *Tectonics* 25:TC6008
- 656 Baldwin JA, Brown M, Schmitz MD (2007) First application of titanium-in-zircon thermometry to ultrahigh-
657 temperature metamorphism. *Geology* 35:295–298
- 658 Ballèvre M, Kienast J-R, Vuichard J-P (1986) La «nappe de la Dent-Blanche» (Alpes occidentales): deux unités
659 austroalpines indépendantes. *Eclogae Geologicae Helvetiae* 79:57–74
- 660 Barboza S, Bergantz G (2000) Metamorphism and Anatexis in the Mafic Complex Contact Aureole, Ivrea Zone,
661 Northern Italy. *Journal of Petrology* 41:1307–1327
- 662 Barboza S, Bergantz G, Brown M (1999) Regional granulite facies metamorphism in the Ivrea zone Is the Mafic
663 Complex the smoking gun or a red herring. *Geology* 27:447–450
- 664 Beltrando M, Rubatto D, Compagnoni R, Lister G (2007) Was the Valaisian basin floored by oceanic crust? Evidence of
665 Permian magmatism in the Versoyen Unit (Valaisian domain, NW Alps). *Ofioliti* 32:85–99
- 666 Bertolani MA (1964) Le metamorfiti dell'alta Valle Strona (Provincia di Novara). *Periodico di Mineralogia* 33:301–336
- 667 Bertotti G, Siletto GB, Spalla MI (1993) Deformation and metamorphism associated with crustal rifting: the Permian to
668 Liassic evolution of the Lake Lugano-Lake Como area (Southern Alps). *Tectonophysics* 226:271–284
- 669 Bertrand JM, Paquette J-L, Guillot F (2005) Permian zircon U-Pb ages in the Gran Paradiso massif: revisiting post-
670 Variscan events in the Western Alps. *Schweizerische Mineralogische und Petrographische Mitteilungen* 85:15–
671 29
- 672 Bigi G, Carozzo MT (1990) Structural model of Italy and gravity map. *Consiglio Nazionale delle Ricerche (Italia)*
673 114:3
- 674 Bosellini A (1991) *Geology of the Dolomites: An Introduction* : Dolomieu Conference on Carbonate Platforms and
675 Dolomitization, Ortisei. Tourist Office
- 676 Bousquet R, Oberhänsli R, Schmid SM, Berger A, Wiederkehr M, Robert C, Rosenberg CL, Koller F, Molli G,
677 Zeilinger G (2012) Metamorphic framework of the Alps CCGM
- 678 Bussy F, Cadoppi P (1996) U-Pb zircon dating of granitoids from the Dora-Maira massif (western Italian Alps).
679 *Schweizerische Mineralogische und Petrographische Mitteilungen* 76:217–233
- 680 Bussy F, Venturini G, Hunziker J, Martinotti G (1998) U-Pb ages of magmatic rocks of the western Austroalpine Dent-
681 Blanche-Sesia unit. *Schweizerische Mineralogische und Petrographische Mitteilungen* 78:163–168
- 682 Bussy F, Hernandez J, von Raumer J (2000) Bimodal magmatism as a consequence of the postcollisional readjustment
683 of the thickened Variscan continental lithosphere (Aiguilles Rouges-Mont Blanc Massifs, Western Alps).
684 *Transactions of the Royal Society of Edinburgh: Earth Sciences* 91:221–233

- 685 Carraro F, Dal Piaz GV, Sacchi R (1970) Serie di Valpelline e II Zona Diorito-Kinzigitica sono i relitti di un
686 ricoprimento proveniente dalla zona Ivrea-Verbanò. *Memorie della Società Geologica Italiana* 9:197–224
- 687 Cassinis G, Toutin-Morin N, Virgili C (1995) A general outline of the Permian continental basins in Southwestern
688 Europe. In: Scholle P et al. (ed) *The Permian of Northern Pangea Volume 2*. Springer, Berlin Heidelberg, pp.
689 137–157
- 690 Cenko-Tok B, Oliot E, Rubatto D, Berger A, Engi M, Janots E, Thomsen TB, Manzotti P, Regis D, Spandler C, Robyr
691 M, Goncalves P (2011) Preservation of Permian allanite within an Alpine eclogite facies shear zone at Mt
692 Mucrone, Italy: Mechanical and chemical behavior of allanite during mylonitization. *Lithos* 125:40–50
- 693 Ciarapica G, Passeri L, Bonetto F, Dal Piaz GV (2016) Facies and Late Triassic fossils in the Roisan zone, Austroalpine
694 Dent Blanche and Mt Mary-Cervino nappe system, NW Alps. *Swiss Journal of Geosciences* 109:1–13
- 695 Compagnoni R (1977) The Sesia-Lanzo Zone: high pressure-low temperature metamorphism in the Austroalpine
696 continental margin. *Rendiconti della Società Italiana di Mineralogia e Petrologia* 33:335–374
- 697 Compagnoni R, Dal Piaz GV, Hunziker J, Gosso G, Lombardo B, Williams P (1977) The Sesia-Lanzo Zone, a slice of
698 continental crust with Alpine high pressure-low temperature assemblages in the Western Italian Alps. *Rendiconti
699 della Società Italiana di Mineralogia e Petrologia* 33:281–334
- 700 Cortiana G, Dal Piaz GV, Del Moro A, Hunziker JC, Martin S (1998) ⁴⁰Ar-³⁹Ar and Rb-Sr dating of the Pillonet klippe
701 and Sesia-Lanzo basal slice in the Ayas valley and evolution of the Austroalpine-Piedmont nappe stack.
702 *Memorie di Scienze Geologiche* 50:177–194
- 703 Dal Piaz GV (1976) Il lembo di ricoprimento del Pillonet (falda della Dent Blanche nelle Alpi occidentali). *Memorie di
704 Scienze Geologiche (Padova)* 31:1–60
- 705 Dal Piaz GV (1999) The Austroalpine-Piedmont nappe stack and the puzzle of Alpine Tethys. *Memorie di Scienze
706 Geologiche* 51:155–176
- 707 Dal Piaz GV, Nervo R (1971) Il lembo di ricoprimento del Glacier-Rafray (Dent Blanche s.l.). *Bollettino della Società
708 Geologica Italiana* 90:401–414
- 709 Dal Piaz GV, Sacchi R (1969) Osservazioni geologiche sul lembo di ricoprimento del Pillonet (Dent Blanche s.l.).
710 *Memorie della Società Geologica Italiana* 10:257–276
- 711 Dal Piaz GV, Cortiana G, Del Moro A, Martin S, Pennacchioni G, Tartarotti P (2001) Tertiary age and paleostructural
712 inferences of the eclogitic imprint in the Austroalpine outliers and Zermatt-Saas ophiolite, western Alps.
713 *International Journal of Earth Sciences* 90:668–684
- 714 Dal Piaz GV, De Vecchi G, Hunziker J (1977) The austroalpine layered gabbros of the Matterhorn and Mt. Collon-
715 Dents de Bertol. *Schweizerische Mineralogische und Petrographische Mitteilungen* 57:59–88
- 716 Dal Piaz GV, Gianotti F, Monopoli B, Pennacchioni G, Tartarotti P, Schiavo A (2010) Note illustrative della Carta
717 Geologica d'Italia alla scala 1: 50.000, Foglio 091 Chatillon. Servizio Geologico d'Italia, Foglio 91:5–152
- 718 Dal Piaz GV, Gosso G, Lombardo B (1983) Metamorphic evolution of the Mt. Emilius klippe, Dent Blanche nappe,
719 western Alps. *American Journal of Science* 283A:438–458
- 720 Dal Piaz GV, Gosso G, Martinotti G (1971) La II Zona Diorito-kinzigitica tra la Valsesia e la Valle d'Ayas (Alpi
721 occidentali). *Memorie della Società Geologica Italiana* 11:433–460
- 722 Dal Piaz GV, Hunziker J, Martinotti G (1972) La Zona Sesia-Lanzo e l'evoluzione tettonico-metamorfica delle Alpi
723 nordoccidentali interne. *Memorie della Società Geologica Italiana* 11:433–466
- 724 De Leo S, Biino G, Compagnoni R (1987) Riequilibrazioni metamorfiche alpine nella serie di Valpelline e di Arolla a
725 Nord di Bionaz (Valpelline-Aosta). *Rendiconti della Società Italiana di Mineralogia e Petrologia* 42:181–182

- 726 Desmons J, Compagnoni R, Cortesogno L, Frey M, Gaggero L (1999) Pre-Alpine metamorphism of the Internal zones
727 of the Western Alps. *Schweizerische Mineralogische und Petrographische Mitteilungen* 79:23–39
- 728 Diehl E, Masson R, Stutz A (1952) Contributo alla conoscenza del ricoprimento della Dent Blanche. *Memorie degli*
729 *Istituti di Geologia e Mineralogia dell'Universita di Padova* 17:1–52
- 730 Diella V, Spalla MI, Tunesi A (1992) Contrasting thermomechanical evolutions in the Southalpine metamorphic
731 basement of the Orobic Alps (Central Alps, Italy). *Journal of Metamorphic Geology* 10:203–219
- 732 Engi M, Scherrer N, Burri T (2001) Metamorphic evolution of pelitic rocks of the Monte Rosa nappe: Constraints from
733 petrology and single grain monazite age data. *Schweizerische Mineralogische und Petrographische Mitteilungen*
734 81:305–328
- 735 Ewing TA, Hermann J, Rubatto D (2013) The robustness of the Zr-in-rutile and Ti-in-zircon thermometers during high-
736 temperature metamorphism (Ivrea-Verbanò Zone, northern Italy). *Contributions to Mineralogy and Petrology*
737 165:757–779
- 738 Ewing TA, Rubatto D, Beltrando M, Hermann J (2015) Constraints on the thermal evolution of the Adriatic margin
739 during Jurassic continental break-up: U-Pb dating of rutile from the Ivrea-Verbanò Zone, Italy. *Contributions to*
740 *Mineralogy and Petrology* 169:1–22
- 741 Fountain D (1976) The Ivrea-Verbanò and Strona-Ceneri Zones, Northern Italy: A cross-section of the continental
742 crust—New evidence from seismic velocities of rock samples. *Tectonophysics* 33:145–165
- 743 Frisch W, Neubauer F (1989) Pre-Alpine terranes and tectonic zoning in the eastern Alps. *Geological Society of*
744 *America, Special Papers* 230:91–100
- 745 Gaidies F, Krenn E, De Capitani C, Abart R (2008a) Coupling forward modelling of garnet growth with monazite
746 geochronology: an application to the Rappold Complex (Austroalpine crystalline basement). *Journal of*
747 *Metamorphic Geology* 26:775–793
- 748 Gaidies F, De Capitani C, Abart R, Schuster R (2008b) Prograde garnet growth along complex P–T–t paths: results
749 from numerical experiments on polyphase garnet from the Wölz Complex (Austroalpine basement).
750 *Contributions to Mineralogy and Petrology* 155:673–688
- 751 Galli A, Le Bayon B, Schmidt M, Burg J-P, Caddick M, Reusser E (2011) Granulites and charnockites of the Gruf
752 Complex: evidence for Permian ultra-high temperature metamorphism in the Central Alps. *Lithos* 124:17–45
- 753 Galli A, Le Bayon B, Schmidt M, Burg J-P, Reusser E, Sergeev S, Larionov A (2012) U-Pb zircon dating of the Gruf
754 Complex: disclosing the late Variscan granulitic lower crust of Europe stranded in the Central Alps.
755 *Contributions to Mineralogy and Petrology* 163:353–378
- 756 Gardien V, Reusser E, Marquer D (1994) Pre-alpine Metamorphic Evolution of the Gneisses From the Valpelline Series
757 (western Alps, Italy). *Schweizerische Mineralogische und Petrographische Mitteilungen* 74:489–502
- 758 Giuntoli F (2016) Assembly of continental fragments during subduction at HP: Metamorphic history of the central Sesia
759 Zone (NW Alps). PhD thesis, University of Bern, Switzerland
- 760 Giuntoli, F., Engi, M. (2016). Internal geometry of the central Sesia Zone (Aosta Valley, Italy): HP tectonic assembly of
761 continental slices. *Swiss Journal of Geosciences* 109:445–471
- 762 Gosso G (1977) Metamorphic evolution and fold history in the eclogitic micaschists of the upper Gressoney valley
763 (Sesia-Lanzo zone, Western Alps). *Rendiconti della Societa Italiana di Mineralogia e Petrologia* 33:389–407
- 764 Gosso G, Messiga B, Rebay G, Spalla M (2010) Interplay between deformation and metamorphism during
765 eclogitization of amphibolites in the Sesia-Lanzo Zone of the Western Alps. *International Geology Review*
766 52:1193–1219

- 767 Grossen N (2012) Polymetamorphic evolution of the Australpine Pillonet Klippe in the Western Alps (Val d'Ayas,
768 Northern Italy). MSc Thesis, University of Bern, Switzerland
- 769 Habler G, Thöni M (2001) Preservation of Permo-Triassic low-pressure assemblages in the Cretaceous high-pressure
770 metamorphic Saualpe crystalline basement (Eastern Alps, Austria). *Journal of Metamorphic Geology* 19:679–
771 697
- 772 Habler G, Thöni M, Grasemann B (2009) Cretaceous metamorphism in the Austroalpine Matsch Unit (Eastern Alps):
773 the interrelation between deformation and chemical equilibration processes. *Mineralogy and Petrology* 97:149–
774 171
- 775 Handy MR, Schmid SM, Bousquet R, Kissling E, Bernoulli D (2010) Reconciling plate-tectonic reconstructions of
776 Alpine Tethys with the geological-geophysical record of spreading and subduction in the Alps. *Earth-Science*
777 *Reviews* 102:121–158
- 778 Hansmann W, Müntener O, Hermann J (2001) U-Pb zircon geochronology of a tholeiitic intrusion and associated
779 migmatites at a continental crust-mantle transition, Val Malenco, Italy. *Schweizerische Mineralogische und*
780 *Petrographische Mitteilungen* 81:239–255
- 781 Harley SL, Kelly NM, Möller A (2007) Zircon Behaviour and the Thermal Histories of Mountain Chains. *Elements*
782 3:25–30
- 783 Harley S (2008) Refining the P–T records of UHT crustal metamorphism. *Journal of Metamorphic Geology* 26:125–
784 154
- 785 Heede H-U (1997) Isotopengeologische Untersuchungen an Gesteinen des ostalpinen Saualpenkristallins, Kärnten.
786 Österreich Münster Forsch Geol Paläont 81:1–168
- 787 Henk A, Franz L, Teufel S, Oncken O (1997). Magmatic Underplating, Extension, and Crustal Reequilibration: Insights
788 from a Cross-Section through the Ivrea Zone and Strona-Ceneri Zone, Northern Italy. *The Journal of Geology*
789 105:367–377
- 790 Hermann J, Rubatto D (2003) Relating zircon and monazite domains to garnet growth zones: age and duration of
791 granulite facies metamorphism in the Val Malenco lower crust. *Journal of Metamorphic Geology* 21:833–852
- 792 Hunziker J (1974) Rb-Sr and K-Ar Age Determination and the Alpine Tectonic History of the Western Alps. *Memorie*
793 *degli Istituti di Geologia e Mineralogia dell'Università di Padova* 31:1–45
- 794 Kiénast JR, Nicot E (1971) Présence d'une paragenese adisthene et chloritoide (d'âge alpin probable) dans les gneiss
795 asillimanite, grenat et cordiérite de Valpelline (Val d'Aoste, Italie). *Comptes Rendus de l'Académie des*
796 *Sciences de Paris, D-272*:1836–1840
- 797 Klötzli US, Sinigoi S, Quick JE, Demarchi G, Tassinari CC, Sato K, Günes Z (2014) Duration of igneous activity in the
798 Sesia Magmatic System and implications for high-temperature metamorphism in the Ivrea-Verbano deep crust.
799 *Lithos* 206–207:19–33
- 800 Köppel V (1974) Isotopic U-Pb ages of monazites and zircons from the crust-mantle transition and adjacent units of the
801 ivrea and ceneri zones (Southern Alps, Italy). *Contributions to Mineralogy and Petrology* 43:55–70
- 802 Kretz R (1983) Symbols for rock-forming minerals. *American Mineralogist* 68:277–279
- 803 Kunz BE, Johnson TE, White RW, Redler C (2014) Partial melting of metabasic rocks in Val Strona di Omegna, Ivrea
804 Zone, northern Italy. *Lithos* 190–191:1–12
- 805 Lardeaux JM (1981) Evolution Tectono-métamorphique de la zone nord du massif de Sésia-Lanzo (Alpes
806 Occidentales): un exemple d'eclogitisation de croûte continentale. Ph.D. dissertation, Université de Paris,
807 Mémoires des Sciences de la Terre, Paris

- 808 Lardeaux JM, Spalla MI (1991) From granulites to eclogites in the Sesia zone (Italian Western Alps): a record of the
809 opening and closure of the Piedmont ocean. *Journal of Metamorphic Geology* 9:35–59
- 810 Lardeaux JM, Gosso G, Kienast JR, Lombardo B (1982) Relations entre le metamorphisme et la deformation dans la
811 zone Sesia-Lanzo (Alpes Occidentales) et le probleme de l'eclogitisation de la croute continentale. *Bulletin de la*
812 *Société géologique de France* 4:793–800
- 813 Lelkes-Felvári G, Frank W, Schuster R (2003) Geochronological constraints of the Variscan, Permian-Triassic and eo-
814 Alpine (Cretaceous) evolution of the great Hungarian Plain Basement. *Geologica Carpathia* 54: 299–315
- 815 Ludwig KR (2003) Isoplot/Ex version 3.0. A geochronological toolkit for Microsoft Excel. Geochronological Centre
816 Special Publication, Berkeley, p 70
- 817 Luvizotto GL, Zack T (2009) Nb and Zr behavior in rutile during high-grade metamorphism and retrogression: An
818 example from the Ivrea-Verbano Zone. *Chemical Geology* 261:303–317
- 819 Mair V, Schuster R, Tropper P (2003) The metamorphic evolution of the Ortler Crystalline. *Mitteilungen der*
820 *Österreichischen Mineralogischen Gesellschaft* 148:215–217
- 821 Manzotti P (2011) Petro-structural map of the Dent Blanche tectonic system between Valpelline and Valtournenche
822 valleys, Western Italian Alps. *Journal of Maps* 7:340–352
- 823 Manzotti P (2012) Polycyclic Evolution in the Dent Blanche Tectonic System. PhD thesis, University of Bern,
824 Switzerland
- 825 Manzotti P, Zucali M (2013) The pre-Alpine tectonic history of the Austroalpine continental basement in the Valpelline
826 unit (Western Italian Alps). *Geological Magazine* 150:153–172
- 827 Manzotti P, Ballèvre MZ, Robyr M, Engi M (2014a) The tectonometamorphic evolution of the Sesia-Dent Blanche
828 nappes (internal Western Alps): review and synthesis. *Swiss Journal of Geosciences* 107:309–336
- 829 Manzotti P, Rubatto D, Darling J, Zucali M, Cenko-Tok B, Engi M (2012) From Permo-Triassic lithospheric thinning to
830 Jurassic rifting at the Adriatic margin: Petrological and geochronological record in Valtournenche (Western
831 Italian Alps). *Lithos* 146–147:276–292
- 832 Manzotti P, Zucali M, Balleve M, Robyr M, Engi M (2014b) Geometry and kinematics of the Roisan-Cignana Shear
833 Zone, and the orogenic evolution of the Dent Blanche Tectonic System (Western Alps). *Swiss Journal of*
834 *Geosciences* 107:1–25
- 835 Marotta AM, Spalla MI (2007) Permian-Triassic high thermal regime in the Alps: Result of late Variscan collapse or
836 continental rifting? Validation by numerical modeling. *Tectonics* 26:TC4016
- 837 Massari F (1988) Some thoughts on the Permo-Triassic evolution of the South-Alpine area. *Memorie della Società*
838 *Geologica Italiana* 34:179–188
- 839 Matte P (1986) Tectonics and plate tectonics model for the Variscan belt of Europe. *Tectonophysics* 126:329–374
- 840 Mayer A, Mezger K, Sinigoi S (2000) New Sm-Nd ages for the Ivrea-Verbano Zone, Sesia and Sessera valleys
841 (Northern-Italy). *Journal of Geodynamics* 30:147–166
- 842 Mehnert KR(1975) The Ivrea Zone: A model of the deep crust. *Neues Jahrbuch Mineralogische Abhandlungen*
843 125:156–199
- 844 Miller C, Thöni M (1997) Eo-Alpine eclogitisation of Permian MORB-type gabbros in the Koralpe (Eastern Alps,
845 Austria): new geochronological, geochemical and petrological data. *Chemical Geology* 137:283–310
- 846 Miller C, Thöni M, Goessler W, Tessadri R (2011) Origin and age of the Eisenkappel gabbro to granite suite (Carinthia,
847 SE Austrian Alps). *Lithos* 125:434–448

- 848 Monjoie P, Bussy F, Schaltegger U, Mulch A, Lapierre H, Pfeifer HR (2007) Contrasting magma types and timing of
849 intrusion in the Permian layered mafic complex of Mont Collon (Western Alps, Valais, Switzerland): evidence
850 from U/Pb zircon and $^{40}\text{Ar}/^{39}\text{Ar}$ amphibole dating. *Swiss Journal of Geosciences* 100:125–135
- 851 Müntener O, Hermann J (1996) The Val Malenco lower crust-upper mantle complex and its field relations (Italian
852 Alps). *Schweizerische Mineralogische und Petrographische Mitteilungen* 76:475–500
- 853 Müntener O, Hermann J (2001) The role of lower crust and continental upper mantle during formation of non-volcanic
854 passive margins: evidence from the Alps. *Geological Society, London, Special Publications* 187:267–288
- 855 Müntener O, Hermann J, Trommsdorff V (2000) Cooling History and Exhumation of Lower-Crustal Granulite and
856 Upper Mantle (Malenco, Eastern Central Alps). *Journal of Petrology* 41:175–200
- 857 Neubauer F, Frisch W, Schmerold R, Schloeser H (1989) Metamorphosed and dismembered ophiolite suites in the
858 basement units of the Eastern Alps. *Tectonophysics* 164:49–62
- 859 Nicot E (1977) Les roches meso et catazonales de la Valpelline (nappe de la Dent Blanche, Alpes italiennes). PhD
860 thesis, Université de Paris VI, France
- 861 Paquette J-L, Chopin C, Peucat J-J (1989) U-Pb zircon, Rb-Sr and Sm-Nd geochronology of high-to very-high-pressure
862 meta-acidic rocks from the Western Alps. *Contributions to Mineralogy and Petrology* 101:280–289
- 863 Peressini G, Quick JE, Sinigoi S, Hofmann AW, Fanning M (2007) Duration of a Large Mafic Intrusion and Heat
864 Transfer in the Lower Crust: a SHRIMP U-Pb Zircon Study in the Ivrea-Verbano Zone (Western Alps, Italy).
865 *Journal of Petrology* 48:1185–1218
- 866 Pesenti C, Zucali M, Manzotti P, Diella V, Risplendente A (2012) Linking U-Th-Pb monazite dating to partial melting
867 microstructures: application to the Valpelline Series (Austroalpine domain, Western Alps). *Rendiconti Online*
868 *Societa Geologica Italiana* 22:183–185
- 869 Petri B (2014) Formation et exhumation des granulites permienes: établir les conditions pré-rift et déterminer l'histoire
870 d'exhumation syn-rift. PhD thesis, University of Strasbourg, France
- 871 Pfiffner A (2009) *Geologie der Alpen*. Haupt Verlag, Bern
- 872 Pognante U, Talarico F, Benna P (1988) Incomplete blueschist re-crytallization in high-grade metamorphics from the
873 Sesia-Lanzo unit (Vasario-Sparone subunit, Western Alps): A case history of metastability. *Lithos* 21:129–142
- 874 Quick JE, Sinigoi S, Mayer A (1995) Emplacement of mantle peridotite in the lower continental crust, Ivrea-Verbano
875 zone, northwest Italy. *Geology* 23:739–742
- 876 Quick JE, Sinigoi S, Peressini G, Demarchi G, Wooden JL, Sbisà A (2009) Magmatic plumbing of a large Permian
877 caldera exposed to a depth of 25 km. *Geology* 37:603–606
- 878 Quick JE, Sinigoi S, Snoke AW, Kalakay TJ, Mayer A, Peressini G (2003) Geologic Map of the Southern Ivrea-
879 Verbano Zone, Northwestern Italy. USGS I-2776:1–22
- 880 Reddy SM, Kelley, SP, Wheeler J (1996) A $^{40}\text{Ar}/^{39}\text{Ar}$ laser probe study of micas from the Sesia Zone, Italian Alps:
881 implications for metamorphic and deformation histories. *Journal of Metamorphic Geology* 14:493–508
- 882 Redler C, Johnson TE, White RW, Kunz BE (2012) Phase equilibrium constraints on a deep crustal metamorphic field
883 gradient: metapelitic rocks from the Ivrea Zone (NW Italy). *Journal of Metamorphic Geology* 30:235–254
- 884 Regis D, Rubatto D, Darling J, Cenki-Tok B, Zucali M, Engi M (2014) Multiple metamorphic stages within an eclogite-
885 facies Terrane (Sesia Zone, Western Alps) revealed by Th-U-Pb petrochronology. *Journal of Petrology* 55:1429–
886 1456

- 887 Ridley J (1989) Structural and metamorphic history of a segment of the Sesia-Lanzo zone, and its bearing on the
888 kinematics of Alpine deformation in the western Alps. *Geological Society, London, Special Publications*
889 45:189–201
- 890 Rivalenti G, Rossi A, Siena F, Sinigoi S (1984) The layered series of the Ivrea-Verbanò igneous complex, western Alps,
891 Italy. *Tschermaks Mineralogische und Petrographische Mitteilungen* 33:77–99
- 892 Roberts MP, Finger F (1997) Do U-Pb zircon ages from granulites reflect peak metamorphic conditions? *Geology*
893 25:319–322
- 894 Robyr M, Darbellay B, Baumgartner LP (2014) Matrix-dependent garnet growth in polymetamorphic rocks of the Sesia
895 zone, Italian Alps. *Journal of Metamorphic Geology* 32:3–24
- 896 Rockenschaub M, Kolenprat B, Frank W (1999) The tectonometamorphic evolution of Austroalpine units in the
897 Brenner area (Tirol, Austria) new geochronological implications. *Tübinger geowissenschaftliche Arbeiten Serie*
898 A 52:118–119
- 899 Rubatto D (2002) Zircon trace element geochemistry: partitioning with garnet and the link between U-Pb ages and
900 metamorphism. *Chemical Geology* 184:123–138
- 901 Rubatto D, Gebauer D, Compagnoni R (1999) Dating of eclogite-facies zircons: the age of Alpine metamorphism in the
902 Sesia-Lanzo Zone (Western Alps). *Earth and Planetary Science Letters* 167:141–158
- 903 Rubatto D, Gebauer D, Fanning M (1998) Jurassic formation and Eocene subduction of the Zermatt-Saas-Fee
904 ophiolites: implications for the geodynamic evolution of the Central and Western Alps. *Contributions to*
905 *Mineralogy and Petrology* 132:269–287
- 906 Rubatto D, Williams IS, Buick IS (2001) Zircon and monazite response to prograde metamorphism in the Reynolds
907 Range, central Australia. *Contributions to Mineralogy and Petrology* 140:458–468
- 908 Sawyer EW (2008) *Atlas of Migmatites*. The Canadian Mineralogist, Special Publications 9, NRC Research Press,
909 Ottawa, Ontario, Canada
- 910 Schaltegger U, Brack P (2007) Crustal-scale magmatic systems during intracontinental strike-slip tectonics: U, Pb and
911 Hf isotopic constraints from Permian magmatic rocks of the Southern Alps. *Contributions to Mineralogy and*
912 *Petrology* 96:1131–1151
- 913 Schaltegger U, Ulianov A, Müntener O, Ovtcharova M, Peytcheva I, Vonlanthen P, Vennemann T, Antognini M,
914 Girlanda F (2015) Megacrystic zircon with planar fractures in miaskite-type nepheline pegmatites formed at high
915 pressures in the lower crust (Ivrea Zone, southern Alps, Switzerland). *American Mineralogist* 100:83–94
- 916 Schmerold R (1988) Die Plankogel-Serie im ostalpinen Kristallin in Kor- und Saualpe (Kärnten-Steiermark-Österreich)
917 als ophiolitische Sutur. PhD thesis, University of Tübingen, Germany
- 918 Schmid R, Wood BJ (1976) Phase relationships in granulitic metapelites from the Ivrea-Verbanò zone (Northern Italy).
919 *Contributions to Mineralogy and Petrology* 54:255-279
- 920 Schmid SM, Fügenschuh B, Kissling E, Schuster R (2004) Tectonic map and overall architecture of the Alpine orogen.
921 *Ecologae Geologicae Helvetiae* 97:93–117
- 922 Schuster R, Frank W (1999) Metamorphic evolution of the Austroalpine units east of the Tauern Window: indications
923 for Jurassic strike slip tectonics. *Mitteilungen der Gesellschaft der Geologie- und Bergbaustudenten in*
924 *Österreich* 42:37–58
- 925 Schuster R, Stüwe K (2008) Permian metamorphic event in the Alps. *Geology* 36:603–606
- 926 Schuster R, Scharbert S, Abart R, Frank W (2001a) Permo-Triassic extension and related HT/LP metamorphism in the
927 Austroalpine-Southalpine realm. *Mitteilungen der Geologie und Bergbaustudenten Österreichs* 45:111–141

- 928 Schuster R, Proyer A, Hoinkes G, Schulz B (2001b) Indications for a Permo-Triassic metamorphic imprint in the
929 Austroalpine crystalline rocks of the Defferegggen Alps (Eastern Tyrol). *Mitteilungen der Österreichischen*
930 *Mineralogischen Gesellschaft* 146
- 931 Schuster R, Tropper P, Krenn E, Finger F, Frank W, Philippitsch R (2015) Prograde Permo-Triassic metamorphic
932 HT/LP assemblages from the Austroalpine Jenig Complex (Carinthia, Austria). *Austrian Journal of Earth*
933 *Sciences* 108:73–90
- 934 Siegesmund S, Layer P, Dunkl I, Vollbrecht A, Steenken A, Wemmer K, Ahrendt H (2008) Exhumation and
935 deformation history of the lower crustal section of the Valstrona di Omega in the Ivrea Zone, southern Alps.
936 *Geological Society, London, Special Publications* 298:45–68
- 937 Sills J (1984) Granulite Facies Metamorphism in the Ivrea Zone, N.W. Italy. *Schweizerische Mineralogische und*
938 *Petrographische Mitteilungen* 64:169–191
- 939 Sinigoi S, Antonini P, Demarchi G, Longinelli A, Mazzucchelli M, Negrini L, Rivalenti G (1991) Intractions of mantle
940 and crustal magmas in the southern part of the Ivrea Zone (Italy). *Contributions to Mineralogy and Petrology*
941 108:385–395
- 942 Sinigoi S, Quick JE, Clemens-Knott D, Mayer A, Demarchi G, Mazzucchelli M, Nehrini L, Rivalenti G (1994)
943 Chemical evolution of a large mafic intrusion in the lower crust, Ivrea-Verbano Zone, northern Italy. *Journal of*
944 *Geophysical Research* 99:21575–21590
- 945 Sinigoi S, Quick JE, Demarchi G, Klötzli U (2011) The role of crustal fertility in the generation of large silicic
946 magmatic systems triggered by intrusion of mantle magma in the deep crust. *Contributions to Mineralogy and*
947 *Petrology* 162:691–707
- 948 Spalla MI, Lardeaux J-M, Dal Piaz GV, Gosso G (1991) Metamorphisme et tectonique a la marge externe de la zone
949 Sesia-Lanzo (Alpes occidentales). *Memorie di Scienze Geologiche* 43:361–369
- 950 Spalla MI, Zanoni D, Marotta A, Rebay G, Roda M, Zucali M, Gosso G (2014). The transition from Variscan collision
951 to continental break-up in the Alps: insights from the comparison between natural data and numerical model
952 predictions. *Geological Society, London, Special Publications* 405:363–400
- 953 Stünitz H (1989) Partitioning of metamorphism and deformation in the boundary region of the "Seconda Zona Diorito-
954 Kinzigitica", Sesia Zone, Western Alps. PhD thesis, ETH Zürich, Switzerland
- 955 Thöni M (1999) A review of geochronological data from the Eastern Alps. *Schweizerische Mineralogische und*
956 *Petrographische Mitteilungen* 79:209–230
- 957 Thöni M, Miller C (2009) The “Permian event” in the Eastern European Alps: Sm-Nd and P–T data recorded by multi-
958 stage garnet from the Plankogel unit. *Chemical Geology* 260: 20–36
- 959 Thöni M, Miller C, Zanetti A, Habler G, Goessler W (2008) Sm-Nd isotope systematics of high-REE accessory
960 minerals and major phases: ID-TIMS, LA-ICP-MS and EPMA data constrain multiple Permian-Triassic
961 pegmatite emplacement in the Koralpe, Eastern Alps. *Chemical Geology* 254:216-237
- 962 Vavra G, Schaltegger U (1999) Post-granulite facies monazite growth and rejuvenation during Permian to Lower
963 Jurassic thermal and fluid events in the Ivrea Zone (Southern Alps). *Contributions to Mineralogy and Petrology*
964 134:405–414
- 965 Vavra G, Gebauer D, Schmid R, Compston W (1996) Multiple zircon growth and recrystallization during polyphase
966 Late Carboniferous to Triassic metamorphism in granulites of the Ivrea Zone (Southern Alps): an ion microprobe
967 (SHRIMP) study. *Contributions to Mineralogy and Petrology* 122:337–358

- 968 Vavra G, Schmid R, Gebauer D (1999) Internal morphology, habit and U-Th-Pb microanalysis of amphibolite-to-
 969 granulite facies zircons: geochronology of the Ivrea Zone (Southern Alps). *Contributions to Mineralogy and*
 970 *Petrology* 134:380–404
- 971 von Raumer JF, Bussy F, Schaltegger U, Schulz B, Stampfli GM (2013) Pre-Mesozoic Alpine basements--their place in
 972 the European Paleozoic framework. *Geological Society of America Bulletin* 125:89–108
- 973 Voshage H, Hofmann AW, Mazzucchelli M, Rivalenti G, Sinigoi S, Raczek I, Demarchi G (1990) Isotopic evidence
 974 from the Ivrea Zone for a hybrid lower crust formed by magmatic underplating. *Nature* 347:731–736
- 975 Vuichard JP (1987) Conditions P–T du métamorphisme anté-alpin dans la «seconde zone dioritokinzigitique» (Zone
 976 Sesia-Lanzo, Alpes occidentales). *Schweizerische Mineralogische und Petrographische Mitteilungen* 67:257–
 977 271
- 978 Vuichard J-P (1989) La marge austroalpine durant la collision alpine : évolution tectonométamorphique de la zone de
 979 Sesia-Lanzo. *Mémoires et Documents du Centre Armoricain d'Etude Structurale des Socles (Rennes)* 24:307
- 980 Watson EB, Wark DA, Thomas, JB (2006) Crystallization thermometers for zircon and rutile. *Contributions to*
 981 *Mineralogy and Petrology* 151:413–433
- 982 Williams P, Compagnoni R (1983) Deformation and metamorphism in the Bard area of the Sesia Lanzo Zone, Western
 983 Alps, during subduction and uplift. *Journal of Metamorphic Geology* 1:117–140
- 984 Yakymchuk C, Brown M (2014) Behaviour of zircon and monazite during crustal melting. *Journal of the Geological*
 985 *Society of London* 171:465–479
- 986 Zanetti A, Mazzucchelli M, Sinigoi S, Giovanardi T, Peressini G, Fanning M (2013) SHRIMP U-Pb Zircon Triassic
 987 Intrusion Age of the Finero Mafic Complex (Ivrea-Verbano Zone, Western Alps) and its Geodynamic
 988 Implications. *Journal of Petrology* 54:2235–2265
- 989 Zingg A (1980) Regional Metamorphism in the Ivrea Zone (Southern Alps, N-Italy): Field and microscopic
 990 Investigations. *Schweizerische Mineralogische und Petrographische Mitteilungen* 60:153–179
- 991 Zucali M (2011) Coronitic microstructures in patchy eclogitised continental crust: the Lago della Vecchia pre-Alpine
 992 metagranite (Sesia-Lanzo Zone, Western Italian Alps). *Journal of the Virtual Explorer* 38:3–28
- 993 Zucali M, Manzotti P, Diella V, Pesenti C, Risplendente A, Darling J, Engi M (2011) Permian tectonometamorphic
 994 evolution of the Dent Blanche Unit (Austroalpine domain, Western Italian Alps). *Rendiconti Online*
 995 *Societa Geologica Italiana* 15:133–136
- 996 Zucali M, Spalla MI, Gosso G (2002) Strain partitioning and fabric evolution as a correlation tool: the example of the
 997 Eclogitic Micaschists Complex in the Sesia-Lanzo Zone (Monte Mucrene-Monte Mars, Western Alps, Italy).
 998 *Schweizerische Mineralogische und Petrographische Mitteilungen* 82:429–454

999

1000

1001 **Figure captions**

1002 **Fig. 1** Geological overview map of the Western and Southern Alps. Sample localities are indicated by stars with
 1003 numbers corresponding to table 1. The South-Alpine domain is subdivided into the Ivrea Zone representing lower
 1004 continental crust levels and the Serie dei Laghi/Strona-Ceneri Zone, which originate from middle to upper crustal
 1005 levels. The Ivrea Zone is further subdivided into the Mafic Complex in purple and the Kinzigite Formation in dark
 1006 brown. The Serie dei Laghi/Strona-Ceneri Zone is subdivided into middle crustal rocks in medium brown and light

1007 brown for upper crustal sediments and volcanics. 2DK – Seconda Zona Dioritico Kinzigitica, EL – Etirol-Levaz Klippe,
1008 EM – Mt. Emilius Klippe, EMC – Eclogitic Micaschist Complex, GMC – Gneiss Minuti Complex, GR – Glacier
1009 Rafray Klippe, MM – Mont Mary nappe, Pil – Pillonet Klippe, RCSZ – Roisan Cignana Shear Zone, V – Verrès Slice.
1010 Map based on Bousquet et al. (2012) and Bigi and Carozzo (1990)

1011

1012 **Fig. 2** Selected field and thin section photographs representative for the high-grade metasediments from the 2DK and
1013 Valpelline Series. **(a)** Migmatite typical of the central 2DK, with distinct leucosome (L) and melanosome (M) domains.
1014 **(b)** Migmatite from the Valpelline Series; L domains interlayered with garnet, biotite and sillimanite schlieren. **(c)** L-
1015 rich migmatite with garnet, sillimanite and biotite in M from the 2DK. **(d)** Garnet-rich migmatite from the Valpelline
1016 Series with schlieren of intergrown biotite and sillimanite. **(e)** Thin section photomicrograph from a M/restite (2DK)
1017 with large garnet porphyroclasts, surrounded by dark-red biotite and prismatic sillimanite; rutile crystals are typically
1018 abundant in restitic parts of these migmatites. **(f)** Thin section photomicrograph from the Valpelline Series with garnet
1019 porphyroclasts surrounded by intergrown prismatic sillimanite and red Ti-rich biotite

1020

1021 **Fig. 3** Select representative zircon CL-images of metapelites except of grain (h), which originates from a grt-leucosome.
1022 **(a–d)** Complex zoned zircon from the EMC with detrital cores, overgrown by up to two Permian rims (CL-dark, CL-
1023 bright) and Alpine overgrowth for (a) and (d). **(e–h)** Zircons representative for the samples from the 2DK. Some
1024 samples/grains preserve detrital cores (e) and (g), while others consist of newly grown metamorphic zircon only (f) and
1025 (h). **(i–m)** Zircon from the Valpelline Series with partially to completely resorbed detrital cores and at least two
1026 generation of Permian metamorphic overgrowth. **(n–s)** Typical zircon textures from the samples of the Mt. Emilius
1027 Klippe. Some grains show mostly detrital cores with thin metamorphic overgrowth (p) and (q), while other samples
1028 show mostly metamorphic growth and non or relic cores only (n), (o), (r) and (s). Scale bar in all images corresponds to
1029 50 μm . A detailed description of the zircon texture for each image is given in the Online Resource 2

1030

1031 **Fig. 4** Probability density plots for U/Pb zircon dates for individual samples from: **(a)** EMC, **(b)** 2DK NE, **(c)** 2DK
1032 central, **(d)** 2DK SW, **(e)** Valpelline Series, and **(f)** Mt. Emilius Klippe. Individual rock samples are colour-coded; n =
1033 number of age data. The individual lines are scaled to their relative abundance of analysed in order to give more weight
1034 to curves with more data points

1035

1036 **Fig. 5 (a)** Probability density plots showing the combined geochronological results for each sample. **(b)** Th/U ratios
1037 plotted against their U/Pb zircon age. Square symbols indicate samples with no to limited HP-overprint; Triangle
1038 symbols indicate samples with pervasive HP-overprint

1039

1040 **Fig. 6 (a)** Ti-concentration in zircon, with corresponding Ti-in-zircon temperatures shown (calibration of Watson et al.
1041 2006). **(b)** Ti-in-zircon concentration plotted against U/Pb age. Diamond symbols: metapelites; Circle symbols:
1042 leucosome; Triangle symbols: HP-overprinted samples; Closed symbols: rutile present; Open symbols: presence of
1043 rutile is unclear or absence

1044

1045 **Fig. 7 (a)** Zr-concentration in rutile with corresponding Zr-in-rutile temperatures (calibration of Watson et al. 2006; zircon
1046 is present in all samples). **(a)** Zr-in-rutile for samples with little to no Alpine overprint from the NE and SW 2DK, as
1047 well as the Valpelline Series. **(b)** Zr-in-rutile for samples with strong Alpine metamorphic overprint from the EMC and
1048 Mt. Emilius Klippe. Diamond symbols: metapelites; Triangle symbols: HP-overprinted samples

1049

1050 **Fig. 8** Summary of Permian metamorphic ages from the Alps

1051

1052 **Fig. 9** Tectonic overview map of the Alps (Schmidt et al. 2004) showing P - T - t data for Permian metamorphism.
1053 References to data presented on the map are given in the text and Online Recourses 3. *Italics* indicate verified contact
1054 metamorphism related to magmatic intrusion

1055

1056 **Table captions**

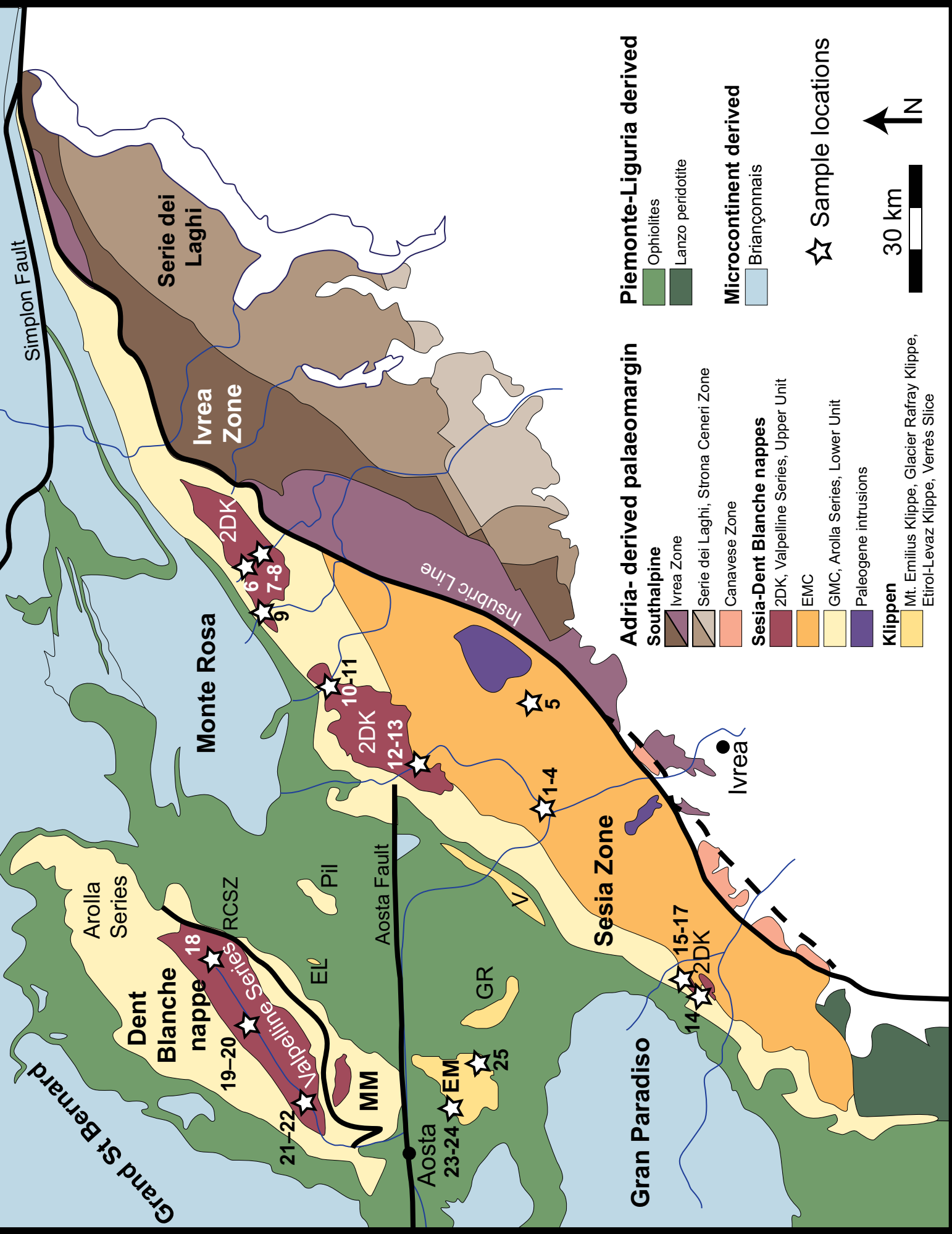
1057 **Tab. 1** List of samples investigated in this study. * partially replaced or altered mineral, ** completely replaced or
1058 altered mineral, only relics or pseudomorphs left

1059

1060 **Tab. 2** Summary table of U/Pb ages, Th-, U-, concentration and Th/U ratios in zircon

1061

1062 **Tab. 3** Summary table of Ti-in-zircon and Zr-in rutile thermometry



Piemonte-Liguria derived

- Ophiolites
- Lanzo peridotite

Microcontinent derived

- Briançonnais

☆ Sample locations

30 km

N

Adria-derived palaeomargin

Southalpine

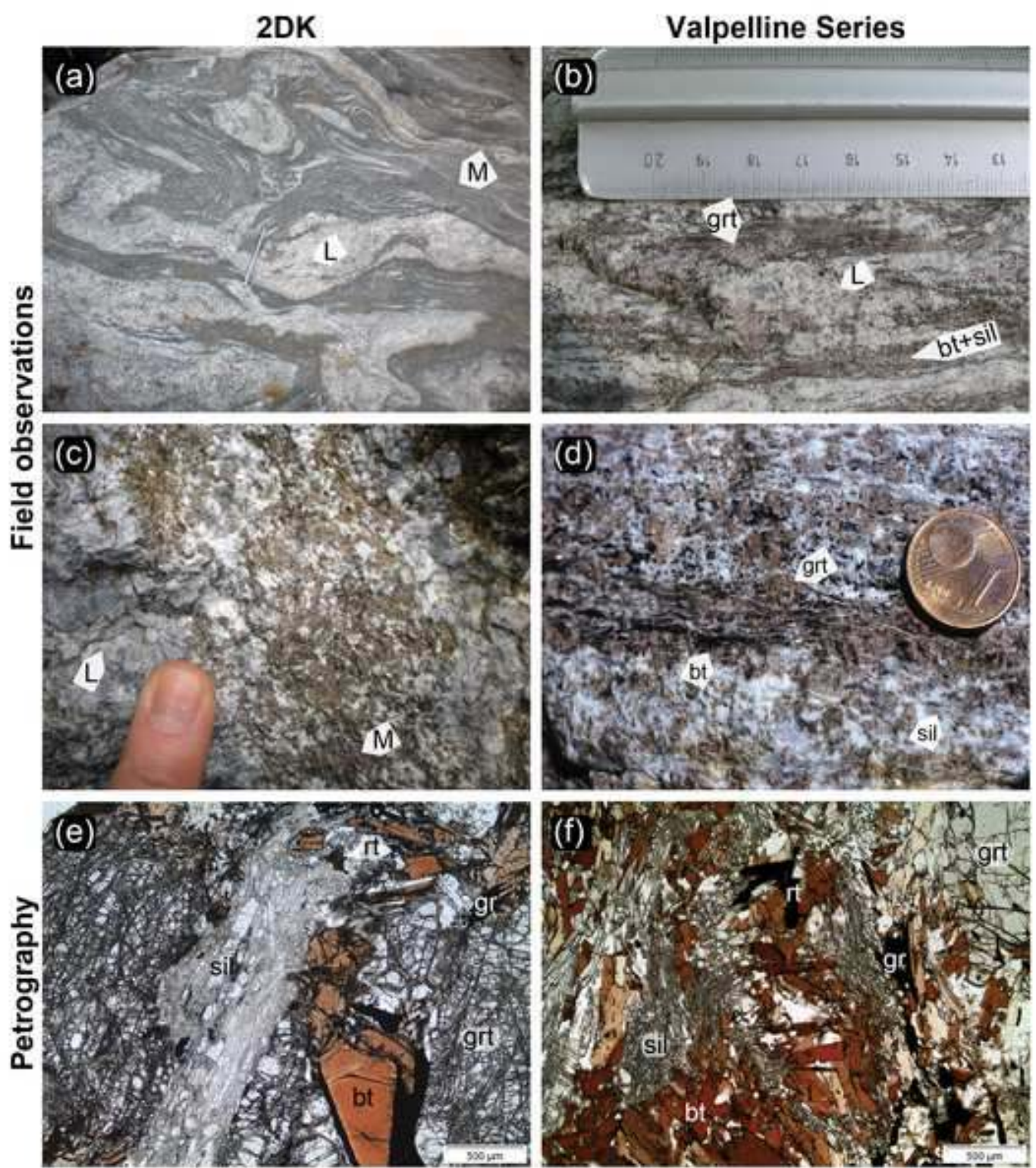
- Ivrea Zone
- Serie dei Laghi, Strona Ceneri Zone
- Canavese Zone

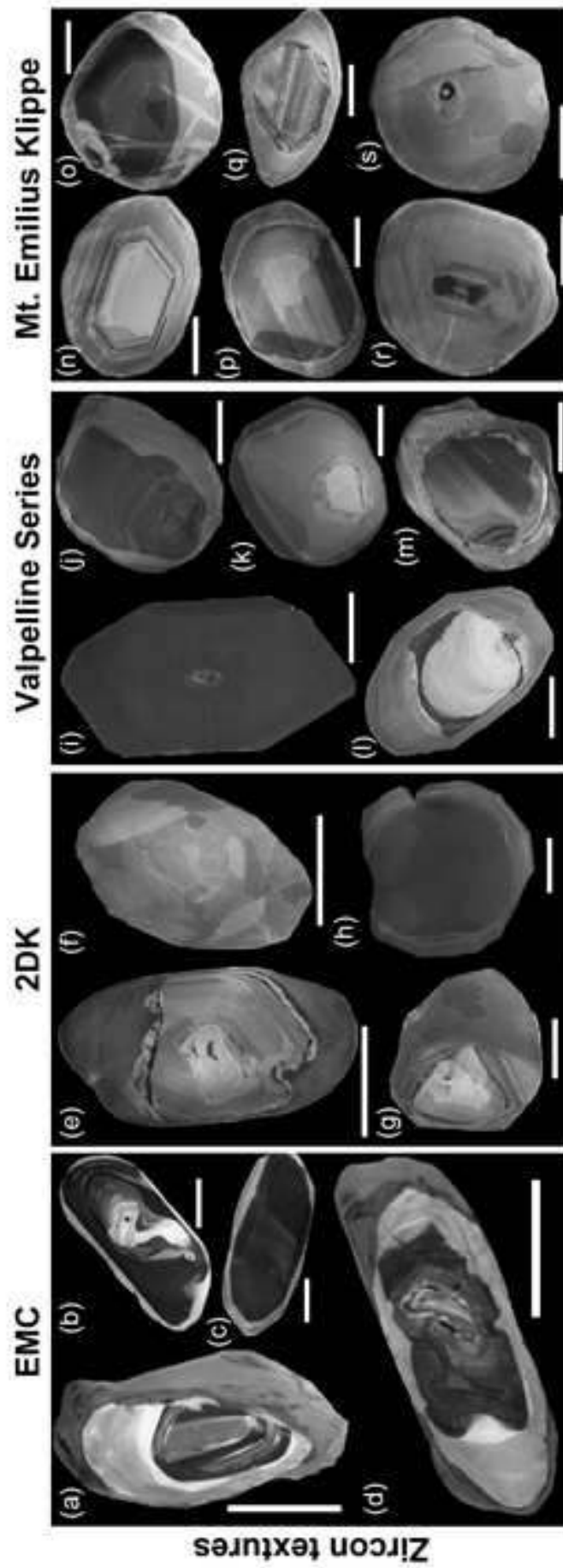
Sesia-Dent Blanche nappes

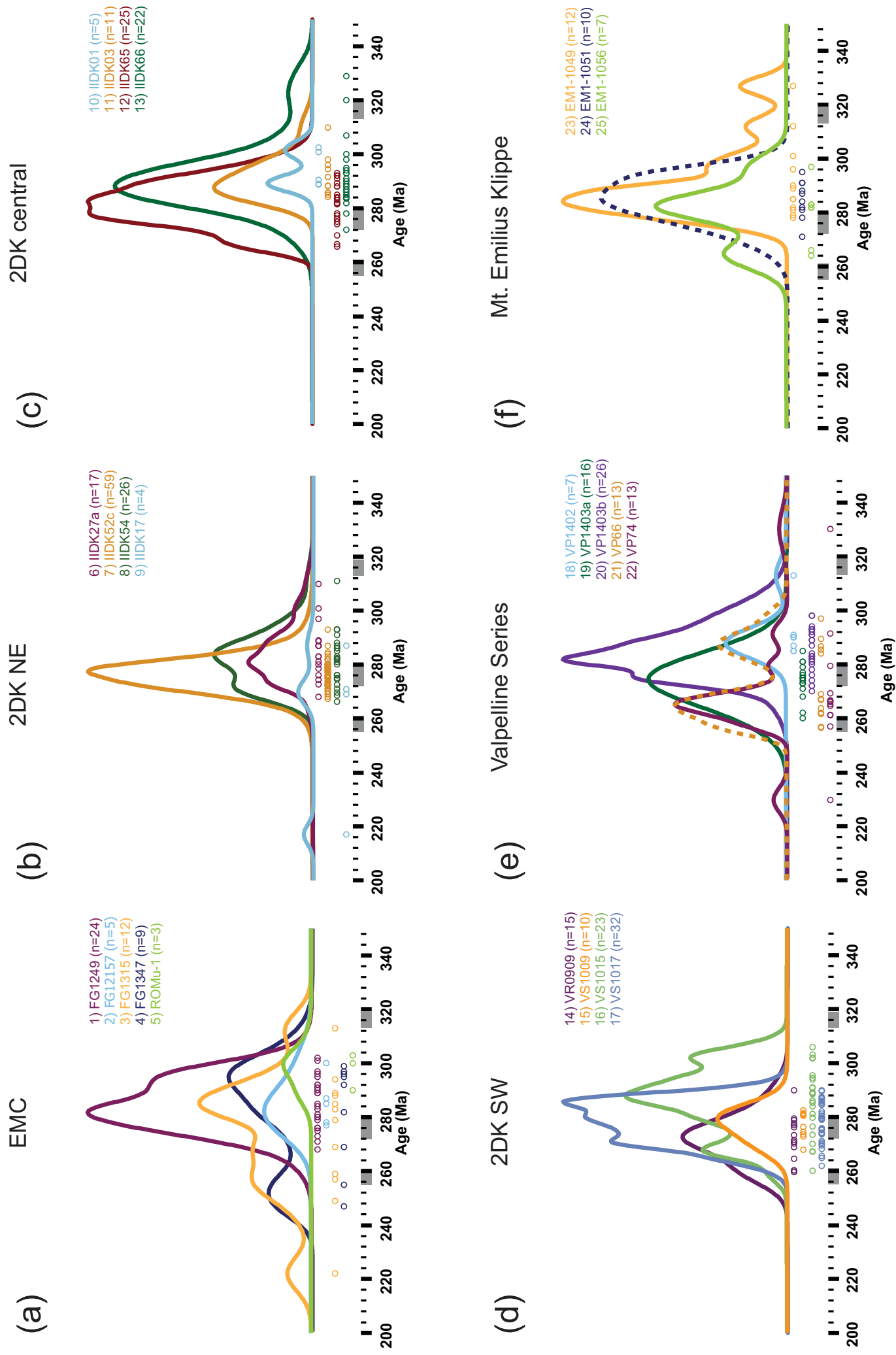
- 2DK, Valpelline Series, Upper Unit
- EMC
- GMC, Arolla Series, Lower Unit
- Paleogene intrusions

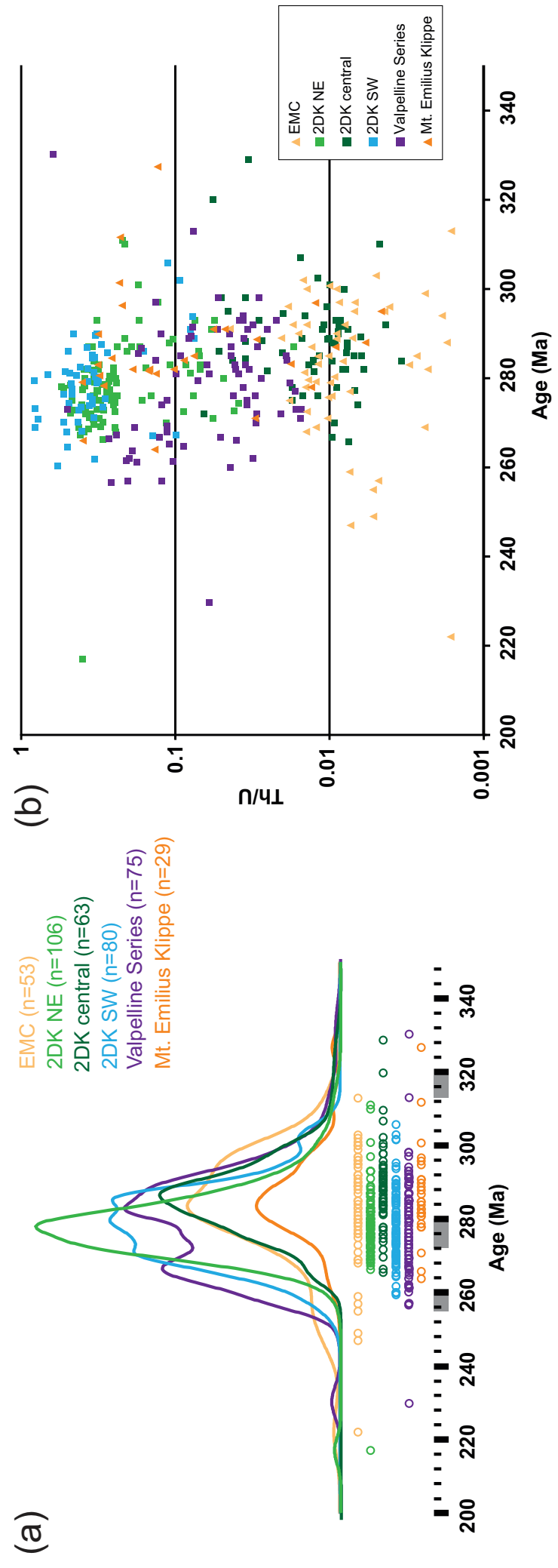
Klippen

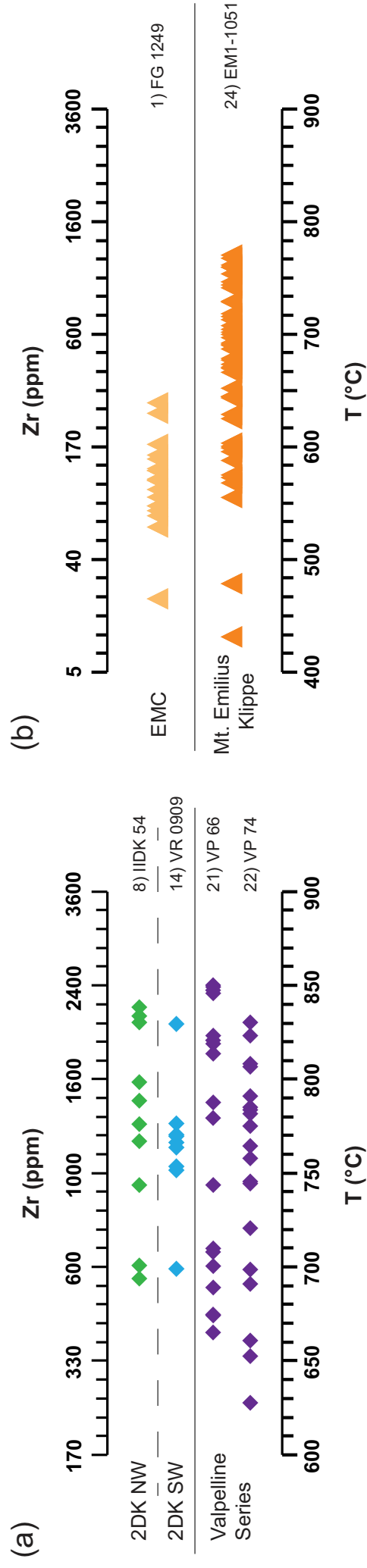
- Mt. Emilius Klippe, Glacier Rafray Klippe, Etirol-Levaz Klippe, Verrès Slice











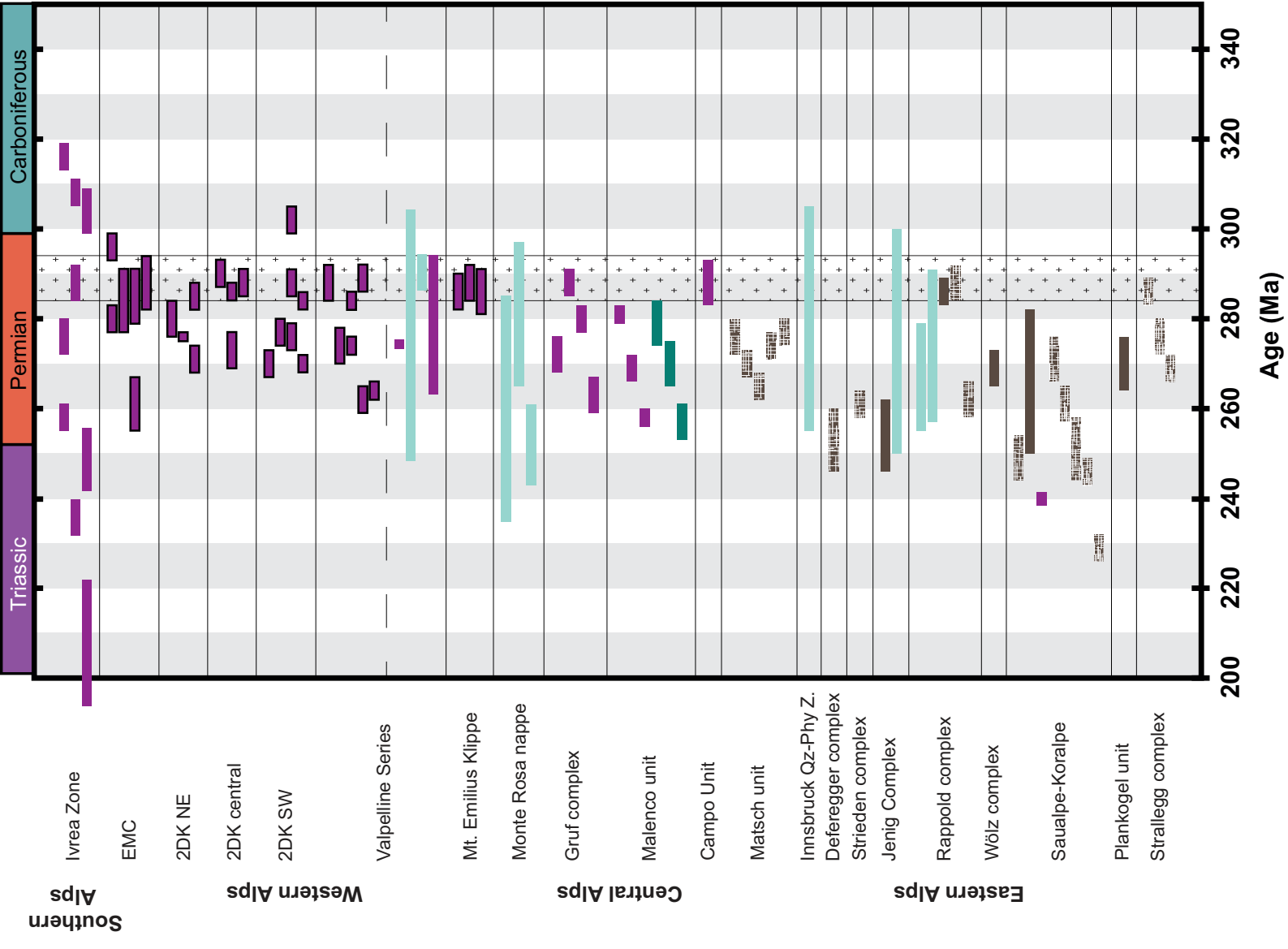


Figure8

Sample	Lithology	Coordinates		Locality	Mineral assemblage	preserved HT Mineral assemblage	Main metamorphic imprint	
		E	N					
EMC								
1	FG 1249	Metasediment	406555	5053733	Faye, Val del Lys	$Ph+Pg+Qtz+Grt+Aln/Ep/Czo+Rt+Gln/Ab/Amp+Zrn$	Grt+Mnz+Zrn	HP
2	FG 12157	Metasediment	409601	5053835	Lillianes, Val del Lys	$Ph+Qtz+Grt+Gln+Ep/Czo/Aln+Chl+Ab+Rt/Tn/Ilm+Grt+Zrn$	Grt+Zrn	HP
3	FG 1315	Metasediment	408432	5051382	Vers-Vert, Val del Lys	$Qtz+Ph+Pg+Grt+Aln/Czo+Chl+Ab/Amp+Rt+Grt+Zrn$	Grt+Mnz+Zrn	HP
4	FG 1347	Metasediment	406236	5052276	Lievanere, Val d'Aosta	$Qtz+Ph+Chl+Grt+Rt+Ep/Czo/Aln+Zrn$	Grt+Mnz+Zrn	HP
5	ROMlu-1	Metasediment	342369	4984896	Laghetto del Monte Rosso	$Qtz+Wm+Grt+Omph+Chl+Ep+Rt+Grt+Zrn$	Zrn	HP
ZDK NE								
6	IIDK 27a	Metapelite	430295	5084906	A. Piana sup., Val Mastallone	$Grt+Wm+Qtz+P^{**}+Kfs^{**}+Sil^{**}+Bt^{**}+Czo+Chl+Zrn+Mnz+Ap+Rt+Ilm$	Grt+Qtz+Pl+Kfs+sSil+Bt+Zrn+Ap+Rt+Ilm	HT
7	IIDK 52c	Leucocratic dyke	433590	5084239	St. Maria, Val Mastallone	$Qtz+Pl+Kfs+Wm+Grt+Bt^{**}+Ep/Czo+Chl+Mnz/Ab/Aln+Rt^{**}+Zrn+Ilm$	Qtz+Pl+Kfs+Grt+Bt+Chl+Mnz+Rt+Zrn+Ilm	HT
8	IIDK 54	Metapelite	432651	5084613	St. Maria, Val Mastallone	$Grt+Qtz+Wm+Bt+P^{**}+Kfs^{**}+Sil+Rt+Ilm+Czo/Ep+Chl+Zrn+Mnz$	Grt+Qtz+Bt+Pl+Kfs+Sil+Rt+Ilm+Zrn+Mnz	HT
9	IIDK 17	Metapelite	426778	5083943	Carcoforo, Val d'Egua	$Qtz+Wm+Chl+Grt^{**}+Rt+Zrn$	Qtz+Grt+Rt+Zrn	GS
ZDK central								
10	IIDK 01	Metapelite	417964	5075679	Riva Valdobbia, Val Sesia	$Qtz+Wm+Grt+Gln+Chl+P^{**}+Kfs^{**}+Bt^{**}+Czo/Ep+Zrn+Tn+Ilm+Py+Gr$	Qtz+Wm+Grt+Pl+Kfs+Bt+Zrn+Ilm+Py+Gr	HT
11	IIDK 03	Leucosome	417964	5075679	Riva Valdobbia, Val Sesia	$Qtz+Wm+Grt+P^{**}+Bt^{**}+Chl+Cz/Ep+Zrn+Tn+Gr$	Qtz+Wm+Grt+Pl+Bt+Zrn+Gr	HT
12	IIDK 65	Metapelite	410936	5065094	Pont Trenta, Val del Lys	$Qtz+Wm+Grt+P^{**}+Kfs^{**}+Bt^{**}+Chl+Czo/Ep+Zrn+Mnz+Tn+Gr$	Qtz+Wm+Grt+Pl+Kfs+Bt+Zrn+Mnz+Gr	HT
13	IIDK 66	Leucosome	410936	5065094	Pont Trenta, Val del Lys	$Qtz+Grt+Wm+P^{**}+Bt^{**}+Chl+Czo/Ep+Zrn+Mnz+Tn$	Qtz+Grt+Wm+Pl+Bt+Zrn+Mnz	HT
ZDK SW								
14	VR 0909	Metapelite	385658	5032740	Vasario, Valle di Ribordone	$Qtz+Grt+Wm+Gln+Pl+Rt+Zrn+Gr+Chl+Czo+Ilm+Tn$	Qtz+Grt+Pl+Rt+Zrn+Gr+Ilm	BS
15	VS 1009	Metapelite	387843	5035282	Ingria, Val Soana	$Pl+Qtz+Wm+Czo+Chl+Tn+Zrn+Ep+Ap+Aln+Rt$	Pl+Qtz+Zrn+Ap+Rt	GS
16	VS 1015	Leucosome	388319	5035497	Ingria, Val Soana	$Wm+Qtz+Czo+Grt+Gln+Pl+Zrn+Aln/Ab/Mnz+Chl+Spn+Rt$	Qtz+Grt+Pl+Zrn+Mnz+Rt	GS
17	VS 1017	Leucosome	388319	5035497	Ingria, Val Soana	$Qtz+Wm+Grt+Bt+Czo+Pl+Tn+Rt+Ap+Amp+Aln+Zrn$	Qtz+Grt+Bt+Pl+Rt+Ap+Zrn	GS
Valpelina Series								
18	VP 1402	Metapelite	383420	5084284	Lac des Placés de Moulin	$Qtz+Grt+Bt+Wm+P^{**}+Chl+Kfs^{**}+Czo/Ep+Zrn+Rt$	Qtz+Grt+Bt+Wm+Pl+Kfs+Zrn+Rt	HT
19	VP 1403a	Restite	376288	5080408	Bionaz, Valpelina	$Grt+Bt+Sil+Pl+Zrn+Chl+Rt$	Grt+Bt+Sil+Pl+Zrn+Rt	HT
20	VP 1403b	Leucosome	376288	5080408	Bionaz, Valpelina	$Qtz+Pl+Kfs+Wm+Czo/Ep+Zrn+Cc+Rt$	Qtz+Pl+Kfs+Wm+Zrn+Rt	HT
21	VP 66	Metapelite	372874	5077575	Thoules, Valpelina	$Pl+Sil+Bt+Qtz+Grt+Rt+Ms+Ep+Zrn+Rt$	Pl+Sil+Bt+Qtz+Grt+Rt+Ms+Zrn+Rt	HT
22	VP 74	Metapelite	372874	5077575	Thoules, Valpelina	$Grt+Bt+Pl+Qtz+Sil+Rt+Ms+Ep+Chl+Zrn+Rt$	Grt+Bt+Pl+Qtz+Sil+Rt+Ms+Zrn+Rt	HT
Mr. Emilius Klippe								
23	EM1-1049	Metasediment	372990	5060520	Becca di Nona	$Qtz+Grt+Wm+Gln+Czo+Chl+Rt+Zrn+Tn$	Grt+Rt+Zrn	HP
24	EM1-1051	Metasediment	372990	5060520	Becca di Nona	$Qtz+Grt+Wm+Chl+Gln+Czo/Ep+Rt+Zrn+Tn$	Grt+Rt+Zrn	HP
25	EM1-1056	Metasediment	374747	5056999	Laghi di Luisset	$Qtz+Wm+Grt+Gln+Rt+Zrn+Ap$	Grt+Rt+Zrn	HP

* partially replaced; ** completely replaced

Table2

Sample	# analyses	Permian dates			Weighted mean age	U (ppm)	Th (ppm)	Th/U	Detrital core dates		
		Max (Ma)	Min (Ma)						# detrital core analyses	Max (Ma)	Min (Ma)
EMC											
1	FG 1249	5	300±17	277±15	294.2±2.8 Ma (MSWD=0.89; n=11); 279.5±2.3 Ma (MSWD=1.14; n=13)	326–868	2–5	0.003–0.014	11	793±20	414±17
2	FG 12157	24	302±14	268±16	285±11 Ma (MSWD=1.3; n=5)	121–1781	2–28	0.007–0.044	–	–	–
3	FG 1315	12	313±13	222±13	285.8±5.6 Ma (MSWD=0.39; n=6)	167–1478	1–5	0.002–0.01	6	696±50	353±25
4	FG 1347	9	299±21	247±11	295.7±7.6 Ma (MSWD=0.068; n=5)	126–1112	0.3–8	0.002–0.012	–	–	–
5	ROMu-1	3	303±14	290±11	297±16 Ma (MSWD=1.4; n=3)	148–1722	0.7–15	0.005–0.009	–	–	–
2DK NE											
6	IIDK 27a	17	310±12	268±13	279.4±3.4 Ma (MSWD=2.0; n=14); 302.6±5.8 Ma (MSWD=1.08; n=3)	156–2050	5–311	0.017–0.296	7	786±26	364±14
7	IIDK 52c	59	293±16	267±6	276.3±1.1 Ma (MSWD=1.3; n=59)	133–664	35–316	0.115–0.550	–	–	–
8	IIDK 54	26	311±14	266±8	285.3±2.7 Ma (MSWD=0.53; n=16); 271.1±2.8 Ma (MSWD=0.54; n=9)	214–1881	26–170	0.056–0.366	9	955±41	544±15
9	IIDK 17	4	287±11	217±7	–	195–295	67–104	0.246–0.399	–	–	–
2DK central											
10	IIDK 01	5	303±7	289±5	301.7±4.4 Ma (MSWD=0.12; n=2); 289.4±3.3 Ma (MSWD=0.102; n=3)	304–729	4–8	0.009–0.012	9	978±20	346±5
11	IIDK 03	11	310±12	284±9	290.7±4.6 Ma (MSWD=2.1; n=11)	105–1260	0.5–20	0.005–0.035	5	1877±95	485±17
12	IIDK 65	25	293±13	266±6	278.7±3.2 Ma (MSWD=4.2; n=25)	393–7800	5–34	0.003–0.025	2	930±40	516±22
13	IIDK 66	22	329±13	272±15	289.4±3.4 Ma (MSWD=1.5; n=20)	316–1609	3–69	0.006–0.065	1	563±23	–
2DK SW											
14	VR 0909	15	290±12	260±13	271.7±4.4 Ma (MSWD=2.1; n=15)	57–109	26–85	0.456–0.819	3	451±16	311±10
15	VS 1009	10	282±13	268±9	277.3±3.1 Ma (MSWD=0.98; n=10)	42–109	20–72	0.41–0.667	–	–	–
16	VS 1015	23	306±7	260±8	302.9±3.1 Ma (MSWD=0.35; n=4); 282.8±4.8 Ma (MSWD=8; n=18)	259–403	25–111	0.076–0.426	3	557±9	380±10
17	VS 1017	32	290±9	262±7	278.4±2.8 Ma (MSWD=8; n=32)	104–359	34–142	0.274–0.4917	–	–	–
Valpelle Series											
18	VP 1402	7	313±11	285±11	288.0±3.9 Ma (MSWD=0.31; n=6)	237–3524	22–176	0.043–0.123	6	672±24	435±11
19	VP 1403a	16	285±17	260±16	273.7±4.1 Ma (MSWD=0.64; n=16)	317–1056	13–259	0.015–0.5	–	–	–
20	VP 1403b	26	298±18	270±16	280.5±2.4 Ma (MSWD=2.8; n=26)	296–2219	8–77	0.019–0.082	–	–	–
21	VP 66	13	297±8	257±6	289.1±6.3 Ma (MSWD=1.4; n=5); 262.7±3.9 Ma (MSWD=1.9; n=8)	206–393	21–88	0.079–0.259	5	507±17	346±14
22	VP 74	13	330±15	230±9	263.9±3.0 Ma (MSWD=1.4; n=9)	79–881	13–108	0.04–0.621	2	1604±84	1073±46
Mt. Emilius Klippe											
23	EM1-1049	12	327±7	278±8	284.9±3.5 Ma (MSWD=1.7; n=8)	121–455	11–144	0.03–0.403	2	932±19	606±12
24	EM1-1051	10	295±7	271±13	286.5±5.4 Ma (MSWD=1.7; n=10)	165–735	1–22	0.005–0.134	11	903±21	455±12
25	EM1-1056	7	297±10	264±10	282.6±5.2 Ma (MSWD=0.015; n=4)	123–730	7–76	0.012–0.398	6	880±32	496±22

Table3

Sample	Ti-in-zrn concentration (ppm)	Ti-in-Zrn temperature (°C)	Zr-in-Rt concentration (ppm)	Zr-in-Rt temperature (°C)
EMC				
1 FG 1249	2.0–2.8	618–641*	4–288	385**–639**
2 FG 12157	–	–	–	–
3 FG 1315	–	–	–	–
4 FG 1347	–	–	–	–
5 ROMu-1	–	–	–	–
2DK NE				
6 IIDK 27a	8.6–15.1	727–778	–	–
7 IIDK 52c	6.3–14.6	707–776	–	–
8 IIDK 54	4.3–11.0	672–749	563–2186	690–840
9 IIDK 17	14.0–25.1	771–829	–	–
2DK central				
10 IIDK 01	2.2–3.8	624–662*	–	–
11 IIDK 03	1.2–4.0	581–666*	–	–
12 IIDK 65	2.3–4.4	628–673*	–	–
13 IIDK 66	1.7–10.5	607–745*	–	–
2DK SW				
14 VR 0909	19.7–43.1	804–888	571–2035	700–830
15 VS 1009	3.7–7.8	660–720	–	–
16 VS 1015	2.3–7.8	627–720	–	–
17 VS 1017	–	–	–	–
Valpeline Series				
18 VP 1402	3.8–7.8	662–719	–	–
19 VP 1403a	4.8–7.3	679–714	–	–
20 VP 1403b	2.9–6.4	642–703	–	–
21 VP 66	2.6–13.5	635–768	400–2395	665–850
22 VP 74	4.1–10.1	669–741	346–2049	630–830
Mt. Emilius Klippe				
23 EM1-1049	4.8–10.6	680–746	–	–
24 EM1-1051	–	–	10–1190	432**–770
25 EM1-1056	11.5–25.9	753–832	–	–

*minimum temperature; no rutile present

**alpine resetting

